Volume 17
Number 1

June *2015*
(ISSN 1109-1606)

# Journal of APPLIED ELECTROMAGNETISM

JAE

Institute of Communication and Computer Systems

Athens - GREECE

Volume 17 June 2015
Number 1 (ISSN 1109-1606)

# JOURNAL OF APPLIED ELECTROMAGNETISM

Institute of Communication and Computer Systems

Athens - GREECE

**Volume 17** **Number 1**

**June 2015**

# TRANS BLACK SEA REGION UNION OF APPLIED ELECTROMAGNETISM (BSUAE)

## JOURNAL OF APPLIED ELECTROMAGNETISM

Institute of Communication and Computer Systems

Athens - GREECE

**Editor: Panayiotis Frangos (Greece),** pfrangos@central.ntua.gr

**Honorary Editor: Nikolaos K. Uzunoglu (Greece), nuzu@central.ntua.gr**

**Board of Associate Editors**

D. Dimitrov (Bulgaria), dcd@tu-sofia.bg
V. Dumbrava (Lithuania), vydum@ktu.lt
G. Georgiev (Bulgaria), gngeorgiev@yahoo.com
G. Matsopoulos (Greece), gmatso@esd.ece.ntua.gr

**Editorial Board**

ALBANIA
G. Bardhyf, bardhylgolemi@live.com
C. Pirro, p_cipo@yahoo.com

ARMENIA
H. Bagdasarian, hovik@seua.sci.am
H. Terzian, hterzian@seua.sci.am

BULGARIA
A. Antonov, asantonov@abv.bg
A. Lazarov, lazarov@bfu.bg
S. Savov, savovsv@yahoo.com

GEORGIA
R. Zaridze, rzaridze@laetsu.org

GERMANY
M. Georgieva – Grosse, mngeorgieva@yahoo.de

GREECE
H. Anastassiu, ANASTASIOU.Christos@haicorp.com
I. Avramopoulos, hav@mail.ntua.gr
G. Fikioris, gfiki@cc.ece.ntua.gr
J. Kanellopoulos, ikanell@cc.ece.ntua.gr
G. Karagiannidis, geokarag@auth.gr
G. Kliros, gsksma@hol.gr
T. Mathiopoulos, mathio@space.noa.gr
C. Moschovitis, harism@noc.ntua.gr
K. Nikita, knikita@cc.ece.ntua.gr
I. Ouranos, iouranos@central.ntua.gr
E. Papkelis, spapkel@central.ntua.gr
J. Sahalos, sahalos@auth.gr
M. Theologou, theolog@cs.ntua.gr

N. Triantafyllou, nitriant@central.ntua.gr
K. Ksystra, katksy@central.ntua.gr
A. Malamou, annamalamou@yahoo.gr

JORDAN
N. Dib, nihad@just.edu.jo

KAZAKSHTAN
S. Sautbekov, sautbek@mail.ru

LITHUANIA
L. Svilainis, linas.svilainis@ktu.lt

RUSSIA
M. Bakunov, bakunov@rf.unn.runnet.ru
A. Grigoriev, adgrigoriev@mail.ru

SERBIA
B. Reljin, ereljin@ubbg.etf.bg.ac.yu

SPAIN
E. Gago – Ribas, egr@tsc.uniovi.es
M. Gonzalez – Morales, gonmor@yllera.tel.uva.es

UNITED KINGDOM
G. Goussetis, G.Goussetis@hw.ac.uk

**Publishing Department**

M. Georgieva – Grosse, mngeorgieva @yahoo.de
N. Triantafyllou, nitriant@central.ntua.gr
K. Ksystra, katksy@central.ntua.gr
A. Malamou, annamalamou@yahoo.gr

# Journal of Applied Electromagnetism

## Copyright Form

**The undersigned I confirm that I agree the publication of the article**

**in the Journal of Applied Electromagnetism and the copyright to belong to Trans Black Sea Union of Applied Electromagnetism. I understand that I have the full right to reuse this manuscript for my own purposes.**

**Name:**

**Surname:**

**Address:**

**E-mail:**

**Signed:**

***Please send the previous form signed either by e-mail to pfrangos@central.ntua.gr , or by fax to the fax number: +30 210 772 2281, attention of Prof. P. Frangos.**

**Address**

Institute of Communication and Computer Systems

National Technical University of Athens

9, Iroon Polytechniou str.

15773 Athens - GREECE

**Tel**: (+30) 2107723694

**Fax**: (+30) 2107722281, attention of Prof. P. Frangos

**e-mail**: pfrangos@central.ntua.gr

**Web site**: **http://jae.ece.ntua.gr**

**TRANS BLACK SEA REGION UNION OF APPLIED ELECTROMAGNETISM (BSUAE)**

**JOURNAL OF APPLIED ELECTROMAGNETISM (JAE)**

**Volume 17 Number 1 June 2015**

**CONTENTS**

**THE METHOD OF AUXILIARY SOURCES FOR THE THIN FILMS SUPERIMPOSED ON THE DIELECTRIC SURFACE**

**I. M. Petoev, V. A. Tabatadze and R. S. Zaridze 1**

*The diffraction problem of the time harmonic electromagnetic wave on the certain metal-dielectric structure was solved by means of the Method of Auxiliary Sources. The structure represents right parallelepiped dielectric. A lattice of thin perfectly conducting films is superimposed on the surface of this dielectric. Selecting the parameters of this structure, in case of resonance between the lattice elements and the dielectric, some interesting properties of the complex materials in wide range of the frequency are revealed. A user friendly computer program has been created for numerical experiments of the stated problem; it gives ability to change the structures' parameters and the incident wave in order to study the properties of these kinds of structures.*

**SCATTERING BY A NIHILITY ELLIPTIC CYLINDER WITH DIELECTRIC COATING AND UNDER LINE SOURCE ILLUMINATION**

**A. K. Hamid 11**

*Scattering by dielectric coated nihility elliptic cylinder is analyzed by solving the analogous problem of scattering by two dielectric layers elliptic cylinder and under line source illumination. The incident, scattered and transmitted fields are expressed in term of Mathieu functions. Numerical results are obtained for the total far fields of dielectric coated nihility strip or elliptic cylinder for different sizes and permittivities.*

**GROUP ANALYSIS OF EQUATIONS OF QUASISTATIONARY ELECTROMAGNETIC FIELD OF HIGH-FREQUENCY INDUCTIVE DISCHARGE OF FINITE LENGTH**

**A. P. Kirpichnikov 21**

*The results of the group analysis of equations of quasi-stationary electromagnetic field of high-frequency inductive discharge of finite length, within the frames of which there have been built Lie algebras of the infinitesimal operators, are given and groups of transformations admitted by the equations of an electromagnetic field in discharge are calculated, and also independent basis scalar invariants (in aggregate forming universal invariants) of these transformation groups are found. The equations of an*

*electromagnetic field written for new variables which scalar invariants of transformation groups are presented.*

**LOW NOISE MICROWAVE AMPLIFIERS WITH IMPROVED INPUT MATCHING APPLICABLE IN ACTIVE ARRAY ANTENNAS**

**M. P. Tonev** **30**

*The difference between the optimal input reflection coefficient for achieving minimal noise figure and those needed for perfect matching is usually a challenge for low noise amplifiers design. Normally amplifiers designed to achieve lowest possible noise figure have very poor input reflection coefficient. This may cause a lot of problems in case of their application as a component in modern active phased array antennas and can be a reason for significant performance degradation. One of the possible solutions is to use balanced amplifier configuration in order to improve input and output matching. The main disadvantages of this solution are degradation of the noise figure due to the losses in the input hybrid and a bigger occupied space.*
*Another approach for solving the problem is presented in this paper. The non – unilateral properties of the transistors are used in order to obtain minimum noise figure and at the same time conjugate matching. Practical circuits and achieved performance are discussed in details.*

**PROVIDING A QUALITY RECEPTION OF DVB-T SIGNALS**

**L. Jordanova, G. Karpov and D. Dobrev** **37**

*The paper deals with the influence of channel coding and modulation, transmitter parameters, distance between transmitter and receiver and propagation losses on the quality of received video information in DVB-T systems. Expressions for calculating of minimum carrier-to-noise ratio at the input of DVB-T receiver, necessary for quasi-error-free reception, are given. Mathematical models to determine the dependence of field strength from distance to DVB-T transmitter are presented. The dependence of minimum mean field strength at the receiver input from CNR is derived and the algorithm for determination of maximum distance to the transmitter is described.*

# The Method of Auxiliary Sources for the Thin Films Superimposed on the Dielectric Surface

I. M. Petoev, V. A. Tabatadze, R. S. Zaridze
Tbilisi State University, Laboratory of Applied Electrodynamics,
3, Chavchavadze Ave. Tbilisi, Georgia
E-mail: ivanpetoev@gmail.com, E-mail: vasilitabatadze@gmail.com,
E-mail: revaz.zaridze@lae.tsu.ge

**Abstract**

*The diffraction problem of the time harmonic electromagnetic wave on the certain metal-dielectric structure was solved by means of the Method of Auxiliary Sources. The structure represents right parallelepiped dielectric. A lattice of thin perfectly conducting films is superimposed on the surface of this dielectric. Selecting the parameters of this structure, in case of resonance between the lattice elements and the dielectric, some interesting properties of the complex materials in wide range of the frequency are revealed. A user friendly computer program has been created for numerical experiments of the stated problem; it gives ability to change the structures' parameters and the incident wave in order to study the properties of these kinds of structures.*

## 1. INTRODUCTION

In the modern micro and nano-electronics, the devices with thin films on the dielectric have wide applications. Therefore, theoretical and numerical study of such structures is a very important problem. In this article, the Method of Auxiliary Sources (MAS) is used, in order to study electromagnetic properties of such structures. It is known, that MAS is efficient for solution of the diffraction problem on the voluminous objects. The application of this method deduced to the construction of two auxiliary surfaces inside and outside of this object.

These surfaces repeat the form of the object and are shifted from the surfaces at the certain distance. The auxiliary sources located on them describe the field in the

opposite parts of divide space. In case of the thin conducting films at the first glimpse the ability of the MAS is restricted, because it is not clear how to distribute the auxiliary surfaces. According to the proposed algorithm the given film should be continued in all direction by imaginary surface at a certain distance. The size of this imaginary surface is one of the auxiliary parameters, which influence the exactness of the calculation. From the both sides of the obtained figure, up and down, there are constructed auxiliary surfaces. Field on top of the film is described by lower auxiliary surface and under the film- by the upper one. The unknown amplitudes of the auxiliary sources on these surfaces are determined by the boundary condition satisfaction, as on the film, also on the imaginary surface. On the both sides of the film tangential component of the total electric film must be zero. The boundary conditions on the imaginary surface are: the tangential component of the electric and magnetic field must be continuous. Results of successful application of described algorithms are provided in [1]. This article is the continuation of the mentioned work. Here, instead of the film in the free media, there is considered a system of such perfectly conducted films, which are superimposed on the surface of an ordinary dielectric.

The motivation in this article is also the will to extend the MAS ability to the solution of such kind of problems efficiently. On the other hand, using the right selection of the resonant parameters of the system, it is desirable to get the effects of multiple resonances [2]. We are looking such resonance frequencies, when both: the film's sizes and the films' lattice parameters in total are resonant together with the dielectric's geometric parameters. Exactly in case of such resonances occur the interesting electromagnetic properties of the study structure, which correspond to the properties of the composite (complex) materials [3, 4, 5].

The numerical calculations were provided using the created user friendly program package. There were found resonant parameters of the system, when it has the properties of the negative refractive index and chirality, in the certain frequency range of the incident field. The results were obtained by parallel validation of the boundary condition satisfaction.

## 2. THEORETICAL PART

**2. 1. Problem statement.** The structure under study represents dielectric parallelepiped with $\varepsilon$ permittivity, on the surface of which is superimposed the lattice of the defined size rectangle conducting films (figure 1). The corners and the vertices of this dielectric are replaced by the cylindrical and spherical surfaces with small radius of curvature, in order to avoid the occurrence of undesirable currents and fields with the singularities on the surfaces.

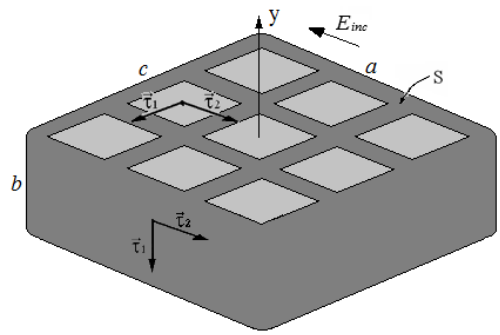


Figure 1. Considered structure
and incident field orientation

This structure is illuminated by a harmonic electromagnetic wave with $e^{-i\omega t}$ time dependence, polarized to the parallel of the films' surface. The electromagnetic wave source can be located outside of the studied structure on certain distance or inside dielectric. Our aim is to find the diffraction field inside and outside of the structure as well as the field in the far zone. The problem consists in the numerical analysis of this scattered field and the character of its polarization, as well as to study the interesting composite materials properties ability of this structure on the resonant frequencies.

**2. 2. Solution of the problem.** A general algorithm for the problem solution is provided below. This algorithm can be used for the more complicate forms of dielectric and the conducting films. Together to the diffraction problem solution it can be considered also as an antenna problem, when the source of the incident field is inside of this structure and we are interested in radiated pattern in far field.

The problem is to find the total inner $\vec{E}_{in}(\vec{r}), \vec{H}_{in}(\vec{r})$ and outer $\vec{E}_{out}(\vec{r})$, $\vec{H}_{out}(\vec{r})$ scattered fields. If the source of incident field is located outside of the structure, then

$$\vec{E}_{out}(\vec{r}) = \vec{E}_1(\vec{r}) + \vec{E}_{inc}(\vec{r}),\ \vec{H}_{out}(\vec{r}) = \vec{H}_1(\vec{r}) + \vec{H}_{inc}(\vec{r}),$$

$$\vec{E}_{in}(\vec{r}) = \vec{E}_2(\vec{r}),\ \vec{H}_{in}(\vec{r}) = \vec{H}_2(\vec{r}).$$

If this source is located inside of the structure, then:

$$\vec{E}_{out}(\vec{r}) = \vec{E}_1(\vec{r}),\ \vec{H}_{out}(\vec{r}) = \vec{H}_1(\vec{r}),$$

$$\vec{E}_{in}(\vec{r}) = \vec{E}_2(\vec{r}) + \vec{E}_{inc}(\vec{r}),\ \vec{H}_{in}(\vec{r}) = \vec{H}_2(\vec{r}) + \vec{H}_{inc}(\vec{r}).$$

Here $\vec{E}_1(\vec{r})$, $\vec{H}_1(\vec{r})$ and $\vec{E}_2(\vec{r})$, $\vec{H}_2(\vec{r})$ are the fields scattered by the structure outside and inside, respectively. Outer and inner total fields should satisfy the boundary conditions on the dielectric $S$ surface and also on the $\sigma$ surface of each conducting plate. On the $S$ surface, total field tangential component continuity is required. From the both side of the conducting films there is required the condition, the tangential component of the total field must be zero. As the problem is 3D, these conditions should be satisfied for any tangential component on the dielectric and conducting surfaces. If they are satisfied along two orthogonal tangential $\vec{\tau}_1$ and $\vec{\tau}_2$ vectors, then it will be satisfied along any other tangential (figure 1)). So:

$$\begin{cases} \vec{E}_{in}(\vec{r}_S)\cdot\vec{\tau}_1 = \vec{E}_{out}(\vec{r}_S)\cdot\vec{\tau}_1, & \vec{H}_{in}(\vec{r}_S)\cdot\vec{\tau}_1 = \vec{H}_{out}(\vec{r}_S)\cdot\vec{\tau}_1, \\ \vec{E}_{in}(\vec{r}_S)\cdot\vec{\tau}_2 = \vec{E}_{out}(\vec{r}_S)\cdot\vec{\tau}_2, & \vec{H}_{in}(\vec{r}_S)\cdot\vec{\tau}_2 = \vec{H}_{out}(\vec{r}_S)\cdot\vec{\tau}_2. \end{cases} \tag{1}$$

Along the conductor surfaces total electric field's tangential component must be zero on the both sides of the pieces:

$$\begin{cases} \vec{E}_{in}(\vec{r}_\sigma)\cdot\vec{\tau}_1 = 0 & \vec{E}_{out}(\vec{r}_\sigma)\cdot\vec{\tau}_1 = 0 \\ \vec{E}_{in}(\vec{r}_\sigma)\cdot\vec{\tau}_2 = 0 & \vec{E}_{out}(\vec{r}_\sigma)\cdot\vec{\tau}_2 = 0 \end{cases}, \tag{2}$$

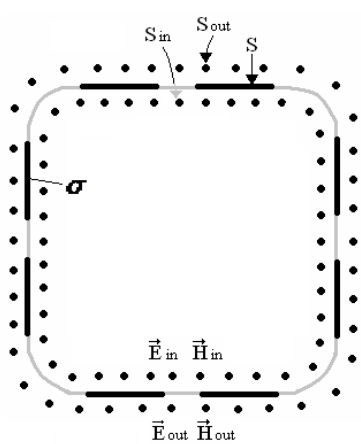


Figure 2. The MAS application

The application of MAS in order to find the fields $\vec{E}_1(\vec{r})$, $\vec{H}_1(\vec{r})$ and $\vec{E}_2(\vec{r})$, $\vec{H}_2(\vec{r})$ is in more details described in the works [2, 6]. The scheme of auxiliary surfaces construction and the distribution of the auxiliary sources on them are presented on the figure 2. So, solution of the problem reduced to the solution of the linear algebraic equations to the unknown amplitudes of auxiliary sources.

## 3. RESULTS OF THE NUMERICAL EXPERIMENTS

**3. 1.Evaluation of the solution accuracy.** Before we get some numerical results it is necessary to be sure that the solution is accurate and we have to determine the error of numerical calculation. For this reason, as examples, we estimate the deviation from the boundary condition satisfaction between the collocation points on the 3 sides of the considered structure, the dimensions of which in the unit of incident wave length is in the given case $0.5\times0.5\times1.3$ (figure 3). Another 3 sides of the object are symmetrical, with the same values. In this case, inner and outer auxiliary surfaces are shifted from the object surface on the distance 0.044 and 0.033 in the unit of the wave length. The provided figures corresponds respectively 16 and 36 collocation points on the squared wave length.

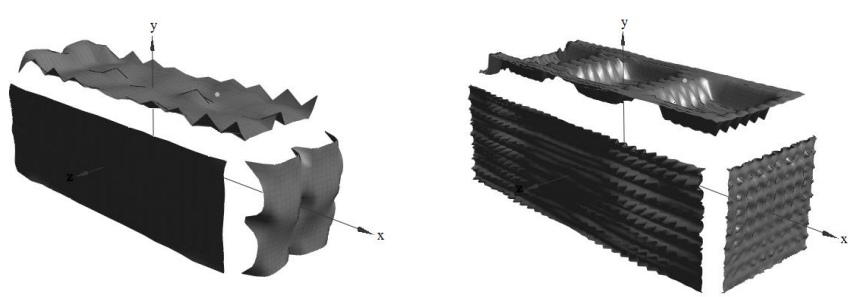


a) b)

Figure 3. The deviation from the boundary condition satisfaction for a) 16 and b) 36 collocation points per wavelength squared

It can be clearly seen that the increase of the collocation points' number decreases the solution error. During numerical experiments and all calculations were done when the boundary conditions deviation was not exceed the 13%, which can be the maximum of the numerical error.

**3.2. The structure with the small number of the films.** An image of the considered structure is presented on the Fig. 4. This structure represents a dielectric object with the permittivity $\varepsilon = 4$, on two opposite sides of which there are superimposed 3 square shape conducted films. The incident field propagates along direction, which makes angle 450 to the X and Y axes, polarized to the parallel of the films surfaces, as it is shown on Fig. 5. Calculations were made to study multiple resonances and to define optimal parameters for complex materials properties of the structure.

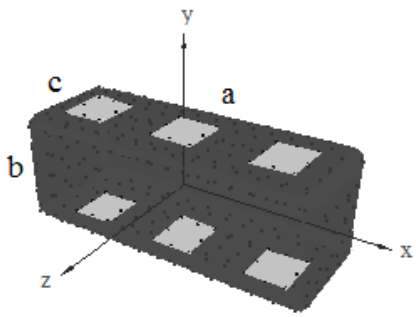


Figure 4. Considered structure

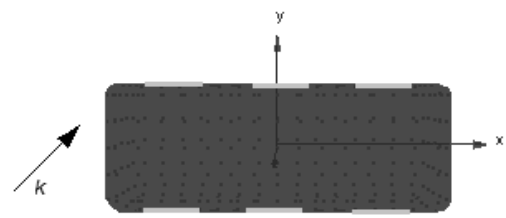


Figure 5. The incident field orientation

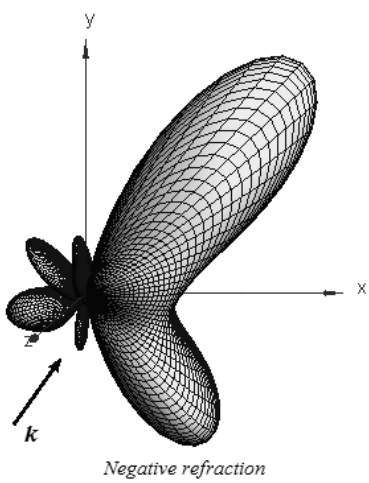


Figure 6. Scattered field in far zone

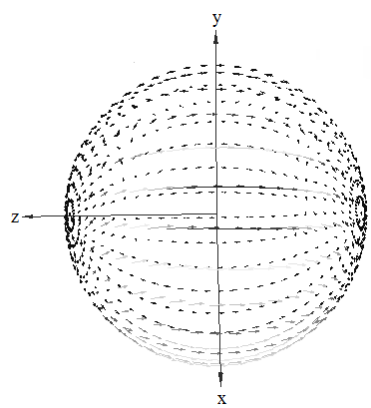


Figure 7. The analysis of the polarization

The numerical calculations showed that in case of the dielectric dimension $a \times b \times c = 0.5 \times 0.5 \times 1.3$ and the size of the film 0.25 (in the units of wavelength), which corresponds to the resonant values, in the pattern of the scattered field appeared an additional lobe, the direction of which corresponds to the negative refraction (figure 6).

Respectively, the given structure with such parameters is similar to the material with negative refractive index. The analysis of the polarization properties of the scattered field showed that along two main lobes it has elliptical polarization with the opposite rotations direction (Fig. 7), which corresponds to the chiral metamaterials. The last one is better seen on the animation. The near total field distribution is given on the Fig. 8.

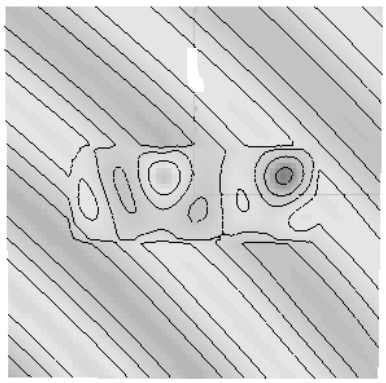

Figure 8. The near total field distribution

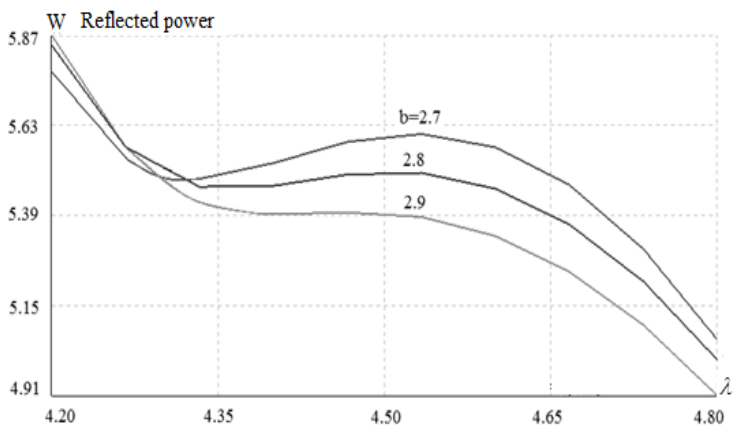


Figure 9. The dependence of the irradiated power on the incident field frequency

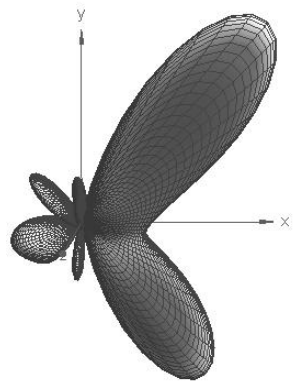


Figure 10. Scattered field in far zone

In order to get the resonance in wider frequency range, the irradiated power dependence on the incident field's frequency in some range, for three different value of the structure's width has been studied. As it is shown on the Fig. 9, in case of the width equal to 2.9 a wider resonance is observed. At that time the negative refracted lobe increased, which corresponds to the increase of this effect Fig. 10. Near field distribution

in two mutual perpendicular sections is shown on the Fig. 11 a) and b). It can be see the resonant (standing) near field inside the structure (Fig.11 b).

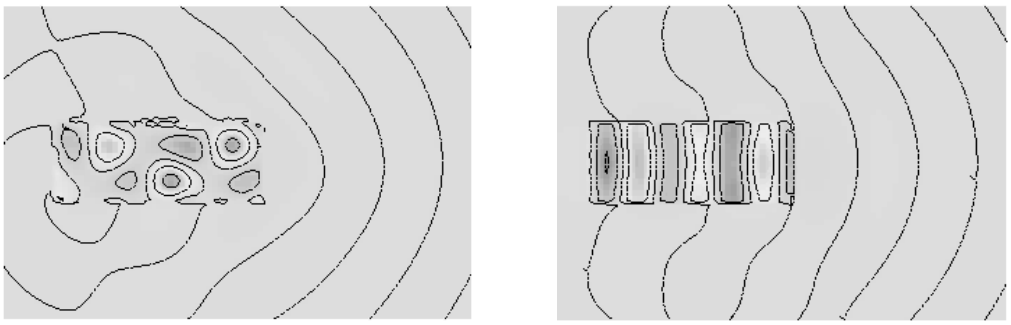

a) b)

Figure 11. Scattered field in far zone:
a) XOY, b) XOZ planes

**3.3. The structure with the big number of the film elements.** In order to increase the effect of negative refraction and chirality, the structure with bigger amount of the film elements, than in the previous case has been considered. On the upper side, as on the lower one we have already 9 films with same sizes and same distance between them (Fig. 12). The dimensions of the dielectric parallelepiped in the units of wavelength are $a \times b \times c = 1 \times 0.35 \times 1$, which yet doesn't correspond to the multiple resonances. Besides this, here we see small lobe of the negative refraction, also the rotation of the polarization is small. The corresponding distribution of the far field pattern and near field in two mutual-perpendicular sections are presented on figures 13, and 14 a), b).

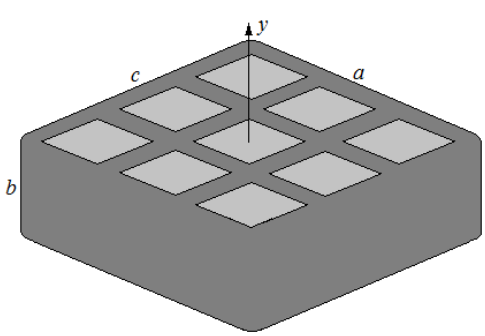


Figure 12. Considered structure

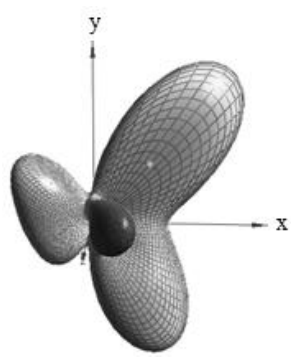


Figure 13. The scattered field in far zone

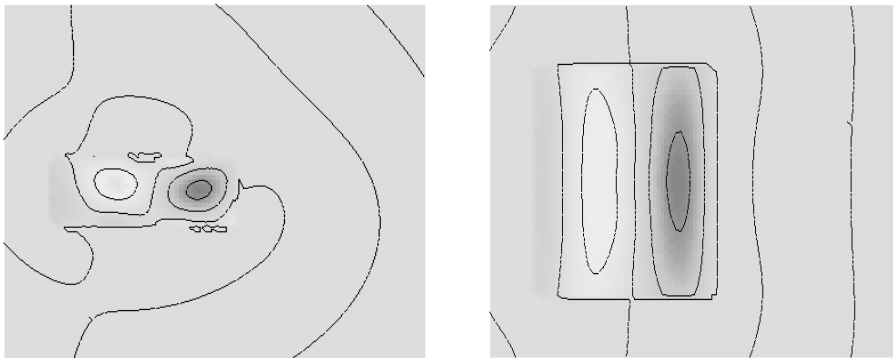

a) b)

Figure 14. Near field distribution: a) XOY and b) XOZ planes

After that there was considered multiple resonant parameters of the structure: $a \times b \times c = 1.33 \times 0.47 \times 1.33$ (in the units of wavelength). In this case, the lobe of negative refraction significantly increased. The corresponding far field pattern and the near field distribution are presented on the Fig. 15 and 16

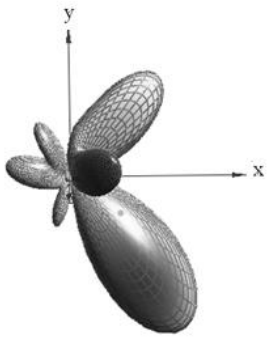


Figure 15. The scattered field in far zone

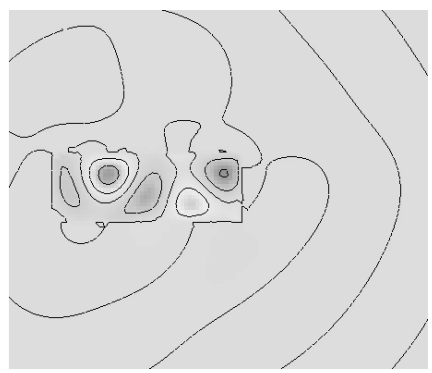

Figure 16. Near scattered field distribution

The animation of the near field shows, that next to the right side of the structure there is the standing wave formed, which takes place in case of multiple resonance.

## 4. CONCLUSION

The interaction of the electromagnetic wave with the dielectric structures, superimposed by the conducting thin plane films, has been studied. Selecting the parameters of the given structures, in case of the resonance between the lattice elements

and the dielectric, there were exposed interesting properties of the negative refraction and the chirality in comparatively wide frequency range. The increase of the film object number increases the resonant effects, which has increased the observed complex materials properties. The numerical calculation was conducted using computer simulation by means of specially created user friendly program package. The method of the problem's numerical solution used the MAS.

## ACKOWLEDGMENT

The work is done with the financial support of the Shota Rustaveli National Science Foundation in the Scope of the grant 52/15.

## REFERENCES

[1] I. Petoev, V. Tabatadze, D. Kakulia, R. Zaridze, "application of the Method of Auxiliary Sources for the thin films and open surfaces" Journal of Communications Technology and Electronics, Moscow, 2014, accepted for publication.

[2] I. Petoev, V. Tabatadze, R. Zaridze, "The Double and Triple Resonances Investigation for the "Cassini" Lattice into the Dielectric". Journal of Applied Electromagnetism (JAE), Vol.15, No. 2, 2013, pp. 8-27.

[3] N. Engheta, R. W. Ziolkowski, "Metamaterials", Physics and Engineering Explorations. John Wiley & Sons, Inc., 2006.

[4] G. V. Eleftheriades, K. G. Balmain, "Negative-Refraction Metamaterials". Fundamental Principles and Applications. Hoboken: John Wiley & Sons, Inc., 2005.

[5] I.V. Lindell, A.H. Sihvola, S.A. Tretyakov, A.J. Viitanen, "Electromagnetic Waves in Chiral and Bi-Isotropic Media". Boston: Artech House, 1994.

[6] I. Petoev, V. Tabatadze, R. Zaridze, "The Method of Auxiliary Sources Applied to Problems of Electromagnetic Wave Diffraction by Certain Metal–Dielectric Structures". Journal of Communications Technology and Electronics, Vol. 58, No. 5, 2013, pp. 404-416.

# Scattering by a Nihility Elliptic Cylinder with Dielectric Coating and Under Line Source Illumination

A. K. Hamid

Department of Electrical and Computer Engineering
University of Sharjah, Box 27272, Sharjah, UAE
akhamid@sharjah.ac.ae

**Abstract**

*Scattering by dielectric coated nihility elliptic cylinder is analyzed by solving the analogous problem of scattering by two dielectric layers elliptic cylinder and under line source illumination. The incident, scattered and transmitted fields are expressed in term of Mathieu functions. Numerical results are obtained for the total far fields of dielectric coated nihility strip or elliptic cylinder for different sizes and permittivities.*

## 1. INTRODUCTION

Analytical solution to the problem of a plane electromagnetic wave scattering by a dielectric coated PEC elliptic cylinder was investigated by many authors [1-2], and the solution is later extended to the nonconfocal dielectric case [3]. Axial slot antenna on a dielectric-coated elliptic cylinder was solved by [4]. Sebak obtained a solution to the problem of scattering from dielectric-coated impedance elliptic cylinder [5]. The scattering by multilayered dielectric elliptic cylinders was studied by many researchers [6-12]. Recently, scattering by nihility circular cylinders and spheres were studied by many authors by letting the refractive index of the dielectric medium approaches zero [13-20].

In this paper, the solution of the electromagnetic wave scattering by a dielectric coated nihility elliptic is obtained by solving the problem of scattering by two dielectric layered elliptic cylinder and letting the refractive index of the inner dielectric layer approaches zero (relative permittivity and relative permeability of the inner medium are approximately null-valued, i.e., the electromagntic waves can not propagate in that region). The analysis and the software used for obtaining the numerical results have been validated, by calculating the total far field for dielectric coated perfectly conducting strip or elliptic cylinder, and showing that these results are in full agreement [21].

## 2. FORMULATION

Consider the case of a line source illumination in the presence of two dielectric layered elliptic cylinder, as shown in Figure 1. The outer dielectric layer has permittivity $\epsilon_1$ and permeability $\mu_1$ while the inner layer is nihility. The semi- major and semi-minor axes are $a$ and $b$ of the nihility layer while $a_1$ and $b_1$ for the dielectric coating.

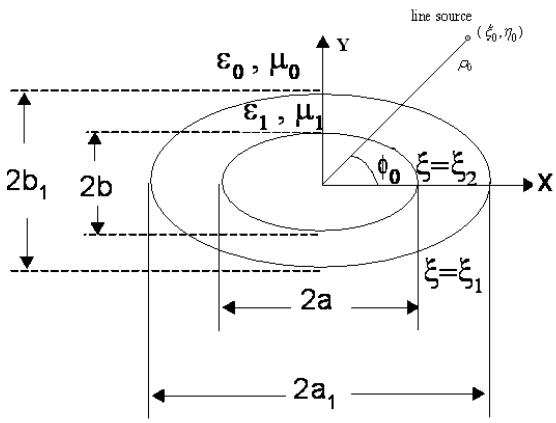


Figure 1. Geometry of the scattering problem.

It is convenient to define the x and y coordinates of the Cartesian coordinate system in terms of u and v coordinates of an elliptical coordinate system also located at the centre of the cylinder in the form of $x = F\cosh u \cos v$ and $y = F\sinh u \sin v$. A time dependence of $e^{jwt}$ is assumed throughout the analysis, but suppressed for convenience. Consider an electric line source parallel to the z-axis and its electric field may be written

$$E_z^i = H_0^{(2)}(k_0 \,|\, \rho - \rho_0 \,|) \tag{1}$$

where $H_0^{(2)}$ is the second kind Hankel function of zero order, and k0 =2 $\pi / \lambda$ 0, with $\lambda$ 0 being the wavelength. The line source electric field may be expanded in terms of angular and radial Mathieu functions as"

$$E_z^i = \sum_{m=0}^{\infty} A_{1em} R_{em}^{(1)}(c_0, \xi) S_{em}(c_0, \eta) + \sum_{m=1}^{\infty} A_{1om} R_{om}^{(1)}(c_0, \xi) S_{om}(c_0, \eta) \;\; \xi_2 < \xi < \xi_0 \tag{2}$$

where

$$A_{\substack{1em\\1om}} = \frac{4\, R^{(4)}_{\substack{em\\om}}(c_0,\xi_0) S_{\substack{em\\om}}(c_0,\eta_0)}{N_{\substack{em\\om}}(c_0)} \tag{3}$$

$$N_{\substack{em\\om}}(c_0) = \int_0^{2\pi} [S_{\substack{em\\om}}(c_0,\eta)]^2 dv \tag{4}$$

$$\xi_0 = \left[ \frac{1}{2}\left(\frac{\rho_0^2}{F^2}+1\right) + \left(\frac{1}{4}\left(\frac{\rho_0^2}{F^2}+1\right)^2 - \frac{x_0^2}{F^2}\right)^{1/2} \right]^{1/2} \tag{5}$$

$$\eta_0 = \frac{x_0}{\xi_0 F} \tag{6}$$

$c_0 = k_0 F$ , F is the semifocal length of the elliptical cross section, $(\xi_o, \eta_o)$ are the elliptic coordinates of the line source. $\xi = \cosh u,\ \eta = \cos v,\ S_{em}$ and $S_{om}$ are the even and odd angular Mathieu functions of order m, respectively, $R^{(1)}_{em}$ and $R^{(1)}_{om}$ are the even and odd radial Mathieu functions of the first kind, $R^{(4)}_{em}$ and $R^{(4)}_{om}$ are the even and odd radial Mathieu functions of the first kind and $N_{em}$ and $N_{om}$ are the even and odd normalized functions.

The scattered electric field outside the multi dielectric layered elliptic cylinder ($\xi > \xi_1$) may be expressed in terms of Mathieu functions as follows:

$$E_z^s = \sum_{m=0}^{\infty} B_{em} R^{(4)}_{em}(c_0,\xi) S_{em}(c_0,\eta) + \sum_{m=1}^{\infty} B_{om} R^{(4)}_{om}(c_0,\xi) S_{om}(c_0,\eta) \tag{7}$$

where $B_{em}$ and $B_{om}$ are the unknown scattered field expansion coefficients. The transmitted electric field into the outer dielectric layer ($\xi_2 < \xi < \xi_1$) may be written as:

$$E_z^I = \sum_{m=0}^{\infty} \left[\ C_{em} R^{(1)}_{em}(c_1,\xi) + D_{em} R^{(2)}_{em}(c_1,\xi)\ \right] S_{em}(c_1,\eta) + \sum_{m=1}^{\infty} \left[\ C_{om} R^{(1)}_{om}(c_1,\xi) + D_{om} R^{(2)}_{om}(c_1,\xi)\ \right] S_{om}(c_1,\eta) \tag{8}$$

where $c_1 = k_1 F$, $k_1 = \omega\sqrt{\mu_1 \varepsilon_1}$, $C_{em}$, $C_{om}$, $D_{em}$, $D_{em}$ are the unknown transmitted field expansion coefficients, and $R_{em}^{(2)}$ and $R_{om}^{(2)}$ are the radial Mathieu functions of the second type.

Similarly, the transmitted electric field into the inner dielectric layer ($\xi < \xi_2$) may be written as:

$$E_z^{II} = \sum_{m=0}^{\infty} F_{em} R_{em}^{(1)}(c_2, \xi) S_{em}(c_2, \eta) + \sum_{m=1}^{\infty} F_{om} R_{om}^{(1)}(c_2, \xi) S_{om}(c_2, \eta) \qquad (9)$$

where $c_2 = k_2 F$, $k_2 = \omega\sqrt{\mu_2 \varepsilon_2}$, and $F_{em}$, $F_{om}$ are the unknown transmitted field expansion coefficients.

The magnetic field components inside and outside the elliptic cylinder can be obtained using Maxwell's equation, i.e.:

$$H_u = \frac{-j}{\omega\mu\, h} \frac{\partial E_z}{\partial v} \qquad (10)$$

$$H_v = \frac{-j}{\omega\mu h} \frac{\partial E_z}{\partial u} \qquad (11)$$

where $h = F\sqrt{\cosh^2 u - \cos^2 v}$. The unknown expansion coefficients in equation (7) can be obtained by imposing the boundary conditions at the various interfaces. Continuity of the tangential field components at $\xi = \xi_1$ and $\xi = \xi_2$ require that:

$$E_z^i + E_z^s = E_z^I \qquad \xi = \xi_1 \qquad (12)$$

$$H_v^i + H_v^s = H_v^I \qquad \xi = \xi_1 \qquad (13)$$

$$E_z^I = E_z^{II} \qquad \xi = \xi_2 \qquad (14)$$

$$H_v^I = H_v^{II} \qquad \xi = \xi_2 \qquad (15)$$

Substituting the appropriate equations into equations (12)-(15) and applying the orthogonality property will lead to a system of equations which may be solved numerically for the unknown scattered field coefficients $B_{\substack{em \\ om}}$.

## 3. NUMERICAL RESULTS

Since the obtained summations constitute the analytic solution, are infinite in extent, to obtain numerical results using a digital computer and the associated software, these summations have to be truncated to include only the first N terms, where N is an integer proportional to the electrical size and the constitutive parameters of the composite object. The results given in this paper have been checked for convergence, and obtained by considering only the first 7 terms (i.e. N = 7) of the infinite series associated with each even and odd function.

The obtained numerical results are presented as total far field for dielectric coated nihility strip or elliptic cylinders of different sizes and permittivities, for both TM and TE polarizations [18]. To validate the analysis and the software used for calculating the results, we have computed the total far field against the scattering angle $\varphi$ of perfectly conducting dielectric coated elliptic cylinder with $\varepsilon_1 = 2.0$, $a = 0.5\lambda$, $a_1 = 0.6\lambda$, $b = 0.0\lambda$, and $b_1 = 0.33\lambda$, $\rho_0 = \lambda$ and $\phi_0 = 90^o$ for TM case [17,21]. The numerical results have been shown in Fig. 2, and they are in full agreement, verifying the accuracy of the analysis as well as the software used for obtaining the results. Also in Fig. 2 shows the total far field for a nihility dielectric coated elliptic cylinder with $\varepsilon_1 = 2.0, 3\ and\ 4$. It can be seen that the total far field is reduced at the scattering angle 90 degrees in the presence of the nihility region while it is increased at the scattering angle 270 degrees. Figure 3 is similar to Figure 2 except for the TE case. It can be seen that the total far field is reduced significantly at the scattering angle 90 degrees in the presence of the nihility region while it is increased significantly the scattering angle 270 degrees. Figure 4 is similar to 2 except for line source location is at $\phi_0 = 0^o$. It can be seen that the total far field is increased at the scattering angle 0 degree and $\varepsilon_1 = 2.0\ and\ 3.0$ while it reduced for $\varepsilon_1 = 4.0$ at the same scattering angle.

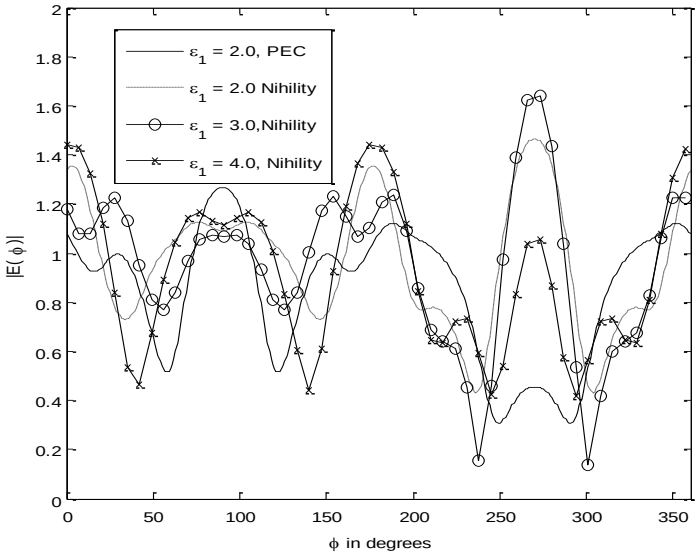


Figure. 2 Total far field against the scattering angle $\varphi$ of nihility dielectric coated elliptic cylinder with $a = 0.5\lambda$, $a_1 = 0.6\lambda$, $b = 0.0\lambda$, and $b_1 = 0.33\lambda$, $\rho_0 = \lambda$ and $\phi_0 = 90^o$, TM case.

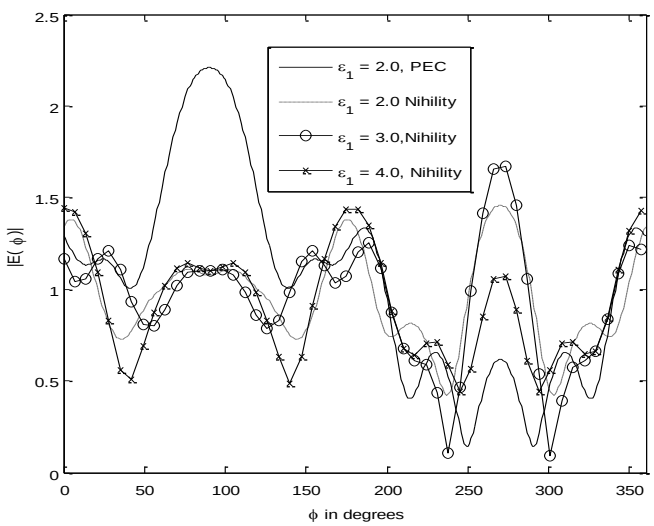


Figure. 3 Total far field against the scattering angle $\phi$ of nihility dielectric coated elliptic cylinder with $a = 0.5\lambda$, $a_1 = 0.6\lambda$, $b = 0.0\lambda$, and $b_1 = 0.33\lambda$, $\rho_0 = \lambda$ and $\phi_0 = 90^o$, TE case.

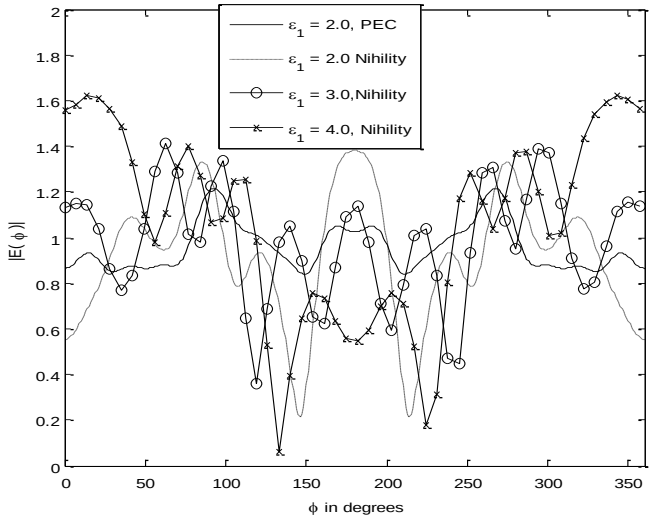


Figure. 4 Total far field against the scattering angle $\phi$ of nihility dielectric coated elliptic cylinder with $a = 0.5\lambda$, $a_1 = 0.6\lambda$, $b = 0.0\lambda$, and $b_1 = 0.33\lambda$, $\rho_0 = \lambda$ and $\phi_0 = 0^o$, TM case.

Fig. 5 Shows total far field against the scattering angle $\varphi$ of nihility dielectric coated elliptic cylinder with $a = 0.5\lambda$, $a_1 = 0.58\lambda$, $b = 0.15\lambda$, and $b_1 = 0.33\lambda$, $\rho_0 = \lambda$ and $\phi_0 = 45^o$, TM case.

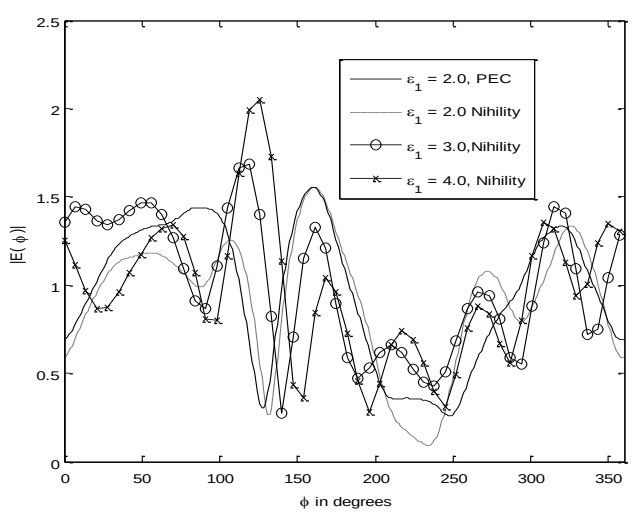


Figure. 5 Total far field against the scattering angle $\phi$ of nihility dielectric coated elliptic cylinder with $a = 0.5\lambda$, $a_1 = 0.58\lambda$, $b = 0.15\lambda$, and $b_1 = 0.33\lambda$, $\rho_0 = \lambda$ and $\phi_0 = 45^o$, TM case.

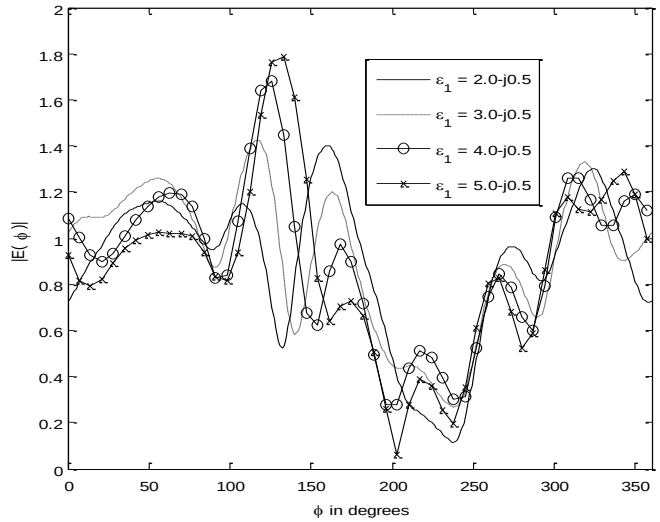


Figure. 6 Total far field against the scattering angle $\phi$ of lossy nihility dielectric coated elliptic cylinder with $a = 0.5\lambda$, $a_1 = 0.58\lambda$, $b = 0.15\lambda$, and $b_1 = 0.33\lambda$, $\rho_0 = \lambda$ and $\phi_0 = 45^o$, TM case.

## 4. CONCLUSIONS

Analytical solution of the electromagnetic wave scattering by nihility dielectric coated elliptic cylinders or strip is obtained for TM and TE polarizations and under line source illumination. The validity and accuracy of the obtained numerical results were verified against the case of dielectric coated perfectly conducting elliptic cylinder or strip and the agreement was excellent. Numerical results were presented as a function of the geometrical parameters of the cylinder and can be used to design scatterers with reduced or enhanced backscattering echo widths. Further, the solution is general where the special case of coated nihility circular cylinder may be obtained by letting the axial ratios approximately equal to 1.0 while the special case of coated nihility strip may be obtained by letting the thickness of the inner cylinder vanishes (letting the minor axis of the inner cylinder approaches zero).

**ACKOWLEDGMENT**

The author wishes to acknowledge the support provided by the University of Sharjah, Sharjah, U.A.E.

## REFERENCES


[1] H. A. Ragheb and L. Shafai, "Electromagnetic scattering from a dielectric coated elliptic cylinder," Can. J. Phys., vol. 66, pp. 1115-1122, 1988.

[2] J.H. Richmond, "Scattering by a conducting elliptic cylinder with dielectric coating," Radio Sci, vol.23, pp. 1061-1066, 1988.

[3] H. A. Ragheb, L. Shafai, and M. Hamid, "Plane wave scattering by a conducting elliptic cylinder coated by a nonconfocal dielectric," IEEE Trans. Antenna and Propag., vol. 39, pp. 218-223, 1991.

[4] J.H. Richmond, "Axial slot antenna on dielectric coated elliptic cylinder," IEEE Trans. Antenna and Propag., vol. 37, pp. 1235-1241, 1989.

[5] A-R. Sebak, "Scattering from dielectric coated impedance elliptic cylinder," IEEE Trans. On Antenna and Progag., vol. 48, pp. 1574-1580, 2000.

[6] R. Holand and V.P. Cable, "Mathieu functions and their applications to scattering by a coated strip," IEEE Trans. On Elect. Compt., vol. 34, no. 1, pp. 9-16, 1992.

[7] S. Caorsi, M. Pastorino, and M. Raffetto, "Electromagnetic scattering by a multilayer elliptic cylinder under transverse-magnetic illumination: series solution in terms of Mathieu function," IEEE Trans. On Antenna and Progag., vol. 45, no. 6, pp. 926-935, 1997.

[8] E. S. Caorsi, M. Pastorino, and M. Raffetto, "Electromagnetic scattering by weakly lossy multilayer elliptic cylinders," IEEE Trans. On Antenna and Progag., vol. 46, no. 11, pp. 1750-1751, 1998.

[9] A. Sebak, L. Shafai, and H. Ragheb, "Electromagnetic scattering by a two layered piecewise homogeneous confocal elliptic cylinder," Radio Science, vol. 26, pp. 111-119, 1991.

[10] A-K. Hamid, **"**Multi-Dielectric Loaded Axially Slotted Antenna on Circular or Elliptic Cylinder," J. of Electromagnetic Waves and Applications, Vol. 20, number 9, pp. 1259-1271, 2006.

[11] A-K. Hamid**, "**Scattering from a Semi-Elliptic Channel in a Ground Plane Loaded by a Lossy or Lossless Dielectric Elliptic Shell", Applied Computational Electromagnetics Society Journal, vol. 22, no. 3, pp. 414-419, 2007.

[12] A-K. Hamid and M.I. Hussein, "Electromagnetic Scattering by a Lossy Dielectric Coated Elliptic Cylinder," Canadian Journal of Physics, Vol. 81, no. 5, pp. 771-778, 2003.

[13] A. Lakhtakia and J.B. Geddes, 'Scattering by a nihility cylinder,' AEÜ International Journal of Electronic and Communications (AEÜ), 61, pp. 62-67, 2007.

[14] A. Lakhtakia, A., 'Scattering by a nihility sphere,' Microwave and Optical Technology Letters, Vol 48, pp. 895 – 896, 2006.

[15] Ahmed, S. and Q. A. Naqvi, "Scattering of Electromagnetic Waves by a Coated Nihility Cylinder", Journal of Infrared, Millimeter and Terahertz Waves,' Vol. 30, Number 10 , PP. 1044-1052, 2009.

[16] Ahmed, S. and Q. A. Naqvi, "Directive EM Radiation of a Line Source in the Presence of a Coated Nihility Cylinder", Journal of Electromagnetic Waves and Applications, Volume 23, Numbers 5-6, 2009 , vol. 11, pp. 761-771, 2009.

[17] A-K. Hamid, "EM Scattering by Nihility Circular or Elliptical Cylinders with Lossy Metamaterials Coating", Journal of International Review on Modelling and Simulations (IREMOS), vol.4, no. 2, pp. 891-895, 2011.

[18] M.H. Hassan, M.J. Mughal, M.M. Ali and Q.A. Naqvi, Electromagnetic fields in a circular waveguide with DBboundary conditions internally coated with chiral-nihility medium, International Journal of Applied Electromagnetics and Mechanics 40, 27–35,2012

[19] M.H. Hassan, M.J. Mughal and A.R. Farooqi, Electromagnetic fields in a circular waveguide with DB_-boundary conditions internally coated with chiral-nihility medium, International Journal of Applied Electromagnetics and Mechanics 40, 301–308, 2012

[20] Muhammad Khalid, Aqeel A. Syed and Qaisar A. Naqvi, Circular cylinder with D'B, DB' and D'B' boundary conditions placed in chiral and chiral nihility media, International Journal of Applied Electromagnetics and Mechanics 44, 59–68, 2014

[21] F. Cooray and A-K. Hamid , "Scattering from a Coated Perfect Electromagnetic Conducting Elliptic Cylinder" International Journal of Electronics and Communications, AEUE, vol. 66, pp. 472-479, 2012.

# GROUP ANALYSIS OF EQUATIONS OF QUASISTATIONARY ELECTROMAGNETIC FIELD OF HIGH-FREQUENCY INDUCTIVE DISCHARGE OF FINITE LENGTH

A. P. Kirpichnikov

Kazan National Research Technological University, Kazan, Russia
K. Marx Str. 68, 420015, Kazan, Russia
e-mail : kirpichnikov@kstu.ru

**Abstract**

*The results of the group analysis of equations of quasi-stationary electromagnetic field of high-frequency inductive discharge of finite length, within the frames of which there have been built Lie algebras of the infinitesimal operators, are given and groups of transformations admitted by the equations of an electromagnetic field in discharge are calculated, and also independent basis scalar invariants (in aggregate forming universal invariants) of these transformation groups are found. The equations of an electromagnetic field written for new variables which scalar invariants of transformation groups are presented.*

## 1. INTRODUCTION

Following the system of designations accepted in the work [1], let us rewrite the full two-dimensional system of equations of an electromagnetic field in discharge [2]

$$\frac{\partial E_\varphi}{\partial r} = -\frac{E_\varphi}{r} + \frac{\omega}{c} H_z \, Sin\left(\varphi_{H_z} - \varphi_{E_\varphi}\right);$$

$$\frac{\partial \varphi_{E_\varphi}}{\partial r} = -\frac{\omega}{c}\frac{H_z}{E_\varphi} Cos\left(\varphi_{H_z} - \varphi_{E_\varphi}\right);$$

$$\frac{\partial H_z}{\partial r} = \frac{\partial H_r}{\partial z} Cos\left(\varphi_{H_z} - \varphi_{H_r}\right) + H_r \frac{\partial \varphi_{H_r}}{\partial z} Sin\left(\varphi_{H_z} - \varphi_{H_r}\right) - \frac{4\pi\sigma}{c} E_\varphi \, Cos\left(\varphi_{H_z} - \varphi_{E_\varphi}\right);$$

$$\frac{\partial \varphi_{H_z}}{\partial r} = -\frac{1}{H_z}\frac{\partial H_r}{\partial z} Sin\left(\varphi_{H_z} - \varphi_{H_r}\right) + \qquad (1)$$

$$+\frac{H_r}{H_z}\frac{\partial\varphi_{H_z}}{\partial z}Cos\left(\varphi_{H_z}-\varphi_{H_r}\right)+\frac{4\pi\sigma}{c}\frac{E_\varphi}{H_z}Sin\,\varphi_{H_z}-\varphi_{E_\varphi};$$

$$\frac{\partial H_r}{\partial r}=-\frac{H_r}{r}-\frac{\partial H_z}{\partial z}Cos\left(\varphi_{H_z}-\varphi_{H_r}\right)+H_z\frac{\partial\varphi_{H_z}}{\partial z}Sin\left(\varphi_{H_z}-\varphi_{H_r}\right);$$

$$\frac{\partial\varphi_{H_r}}{\partial r}=-\frac{1}{r}\frac{\partial H_z}{\partial z}Sin\left(\varphi_{H_z}-\varphi_{H_r}\right)-\frac{H_z}{H_r}\frac{\partial\varphi_{H_z}}{\partial z}Cos\left(\varphi_{H_z}-\varphi_{H_r}\right),$$

as

$$u_1=-\frac{u}{r}+\alpha\,v\,Sin\left(y-x\right);$$

$$x_1=-\alpha\frac{v}{u}Cos\left(y-x\right);$$

$$v_1=w_2\,Cos\left(y-z\right)+w\,z_2\,Sin\left(y-z\right)-\beta\,u\,Cos\left(y-x\right);$$

$$y_1=-\frac{w_2}{v}Sin\left(y-z\right)+\frac{w}{v}z_2\,Cos\left(y-z\right)+\beta\frac{u}{v}Sin\left(y-x\right); \qquad (2)$$

$$w_1=-\frac{w}{r}-v_2\,Cos\left(y-z\right)+v\,y_2\,Sin\left(y-z\right);$$

$$z_1=-\frac{v_2}{w}Sin\left(y-z\right)-\frac{v}{w}y_2\,Cos\left(y-z\right).$$

In the equations (1), $E_\varphi$, $\varphi_{E_\varphi}$, $H_z$, $\varphi_{H_z}$, $H_r$, $\varphi_{H_r}$ are the amplitude value and circuit angle of electric curl, longitudinal and cross-magnetized fields within plasmoid respectively; $\sigma$-conductivity in discharge; $\omega$ - oscillation frequency of a HF field; *c*- speed of light in a vacuum in Gaussian system of units. In the equations (2) and the following formulae according to [1] $t=z$; $u=E_\varphi$; $v=H_z$; $w=H_r$; $x=\varphi_{E_\varphi}$; $y=\varphi_{H_z}$ and $z=\varphi_{H_r}$; $\alpha=\omega/c$; $\beta=4\pi\sigma/c$; index “1” designates radial derivatives of corresponding values, index “2 “ – axial ones.

## 2. TWO-DIMENSIONAL MODEL OF HFI DISCHARGE

The system (2) written in this way admits three-dimensional Lie algebra $L^3$ of the infinitesimal operators the basis of which in a finite-dimensional solutions space of constitutive equations takes the form

$$X_1 = \frac{\partial}{\partial t};$$

$$X_2 = u\frac{\partial}{\partial u} + v\frac{\partial}{\partial v} + w\frac{\partial}{\partial w}; \tag{3}$$

$$X_3 = \frac{\partial}{\partial x} + \frac{\partial}{\partial y} + \frac{\partial}{\partial z},$$

to which the table of generators satisfies

| | $\tilde{t}$ | $\tilde{u}$ | $\tilde{x}$ | $\tilde{v}$ | $\tilde{y}$ | $\tilde{w}$ | $\tilde{z}$ | $\tilde{r}$ |
|---|---|---|---|---|---|---|---|---|
| $X_1$ | 1 | 0 | 0 | 0 | 0 | 0 | 0 | 0 |
| $X_2$ | 0 | $u$ | 0 | $v$ | 0 | $w$ | 0 | 0 |
| $X_3$ | 0 | 0 | 1 | 0 | 1 | 0 | 1 | 0 |

(in the tables the coordinates of operators are designated by the same letters as variables but with a wave on their top).

The three-parametric Abelian (commutative) group $G^3$ of the following transformations corresponds to the system of basis operators (3):

$r' = r$ (identity transformation);

$t' = t + a_1$ (parallel transfer); (4)

$u' = u\exp(a_2)$; $v' = v\exp(a_2)$; $w' = w\exp(a_2)$ (dilation and compression group);

$x' = x + a_3$; $y' = y + a_3$; $z' = z + a_3$ (the group of parallel transfers)

($a_1$, $a_2$, и $a_3$ – parameters of the group).

It is obvious that in total there are 8-3=5 independent basis scalar invariants of the group (4) which in aggregate forms a universal invariant

$$J = \left( r, \frac{u}{v}, \frac{w}{v}, y - x, y - z \right)$$

or, in normal designations (in physical variables),

$$J = \left( r, \frac{E_\varphi}{H_z}, \frac{H_r}{H_z}, \varphi_{H_z} - \varphi_{E_\varphi}, \varphi_{H_z} - \varphi_{H_r} \right).$$

## 3. ONE-DIMENSIONAL MODEL OF HFI DISCHARGE

In the same system of designation, the equations of electromagnetic field in a one-dimensional statement of the problem, obviously, takes the form

$$\frac{\partial E_\varphi}{\partial r} = -\frac{E_\varphi}{r} + \frac{\omega}{c} H_z \, Sin\left(\varphi_{H_z} - \varphi_{E_\varphi}\right);$$

$$\frac{\partial \varphi_{E_\varphi}}{\partial r} = -\frac{\omega}{c} \frac{H_z}{E_\varphi} Cos\left(\varphi_{H_z} - \varphi_{E_\varphi}\right);$$

$$\frac{\partial H_z}{\partial r} = -\frac{4\pi\sigma}{c} E_\varphi \, Cos\left(\varphi_{H_z} - \varphi_{E_\varphi}\right); \tag{5}$$

$$\frac{\partial \varphi_{H_z}}{\partial r} = \frac{4\pi\sigma}{c} \frac{E_\varphi}{H_z} Sin\left(\varphi_{H_z} - \varphi_{E_\varphi}\right)$$

or

$$u_1 = -\frac{u}{r} + \alpha \, v \, Sin\left(y - x\right);$$

$$x_1 = -\alpha \frac{v}{u} Cos\left(y - x\right);$$

$$v_1 = -\beta \, u \, Cos\left(y - x\right);$$

$$y_1 = +\beta \frac{u}{v} Sin\left(y - x\right).$$

This system also admits three-dimensional Lie algebra $L^3$, to the basis vectors of which

$$X_1 = \frac{\partial}{\partial t};$$

$$X_2 = u\frac{\partial}{\partial u} + v\frac{\partial}{\partial v};$$

$$X_3 = \frac{\partial}{\partial x} + \frac{\partial}{\partial y}$$

the table of operators corresponds

| | $\tilde{t}$ | $\tilde{u}$ | $\tilde{x}$ | $\tilde{v}$ | $\tilde{y}$ | $\tilde{r}$ |
|---|---|---|---|---|---|---|
| $X_1$ | 1 | 0 | 0 | 0 | 0 | 0 |
| $X_2$ | 0 | $u$ | 0 | $v$ | 0 | 0 |
| $X_3$ | 0 | 0 | 1 | 0 | 1 | 0 |

Specified basis operators respond the three-parametric Abelian group $G^3$ consisting of transformations:

$r' = r$ (identity transformation);

$t' = t + a_1$ (parallel transfer); (6)

$u' = u\exp(a_2)$; $v' = v\exp(a_2)$ (dilation and compression group);

$x' = x + a_3$; $y' = y + a_3$ (group of parallel transfers)

($a_1$, $a_2$ и $a_3$ – parameters of the group).

There are 6-3=3 independent basis scalar invariants of the group (6) that form its universal invariant

$$J = \left(r, \frac{u}{v}, y - x\right)$$

or

$$J = \left( r, \frac{E_\varphi}{H_z}, \varphi_{H_z} - \varphi_{E_\varphi} \right).$$

## 4. MODEL OF HFI DISCHARGE IN NEAR-AXIAL ZONES OF PLASMIC TORCH

And, at last, let us consider equations describing the structure of quasistationary electromagnetic field of HFI discharge of finite length in near-axial zones of plasmoid, i.e. system [3, 4]

$$\frac{\partial H_z}{\partial r} - \frac{\partial H_r}{\partial z} = a\, H_z(0,z)\, r^3;$$

$$\frac{1}{r}\frac{\partial}{\partial r}(rH_r) + \frac{\partial H_z}{\partial z} = 0,$$

in which $a = \omega^2\, \pi^2\, \sigma^2(0,z)/c^4$, having the exact analytical decision [3]

$$H_z(r,\mathrm{z}) = H_z(0,0)\left\{ I_0(br) + \frac{64a^2}{b^4}\left[ I_0(br) - 1 - \frac{b^2 r^2}{4} \right] \right\} Cos(bz),;$$

$$H_r(\mathrm{r,z}) = H_z(0,0)\left\{ I_1(br) + \frac{64a^2}{b^4}\left[ I_1(br) - \frac{br}{2} - \frac{b^3 r^3}{16} \right] \right\} Sin(bz),$$

written by means of modified Bessel functions $I_0$ and $I_1$ of zero and first orders, parameter $b = \frac{1}{L}\arccos\left[\frac{H_z(0,L)}{H_z(0,0)}\right]$, where *L*- the length of an estimated area on the coordinate *z*, digitized from the central section of a plasmoid. In our designations it will be the system

$$v_1 - w_2 = a\, v(0,z)\, r^3;$$

$$w_1 + \frac{w}{r} = -v_2.$$

Admitted Lie algebra $L^2$ in this case is two-dimensional, its basis operators are as follows

$$X_1 = \frac{\partial}{\partial t}$$

and

$$X_2 = v\frac{\partial}{\partial v} + w\frac{\partial}{\partial w}.$$

The table of these operators:

| | $\tilde{t}$ | $\tilde{v}$ | $\tilde{w}$ | $\tilde{r}$ |
|---|---|---|---|---|
| $X_1$ | 1 | 0 | 0 | 0 |
| $X_2$ | 0 | $v$ | $w$ | 0 |

Basis operators respond to the two-parameter Abelian group of transformations $G^2$:

$r' = r$ (identity transformation);

$t' = t + a_1$ (parallel transfer); (7)

$v' = v\exp(a_2)$; $w' = w\exp(a_2)$ (dilation and compression group)

($a_1$, $a_2$ – parameters of the group).

It is obvious that there are 4-2=2 independent basis scalar invariants of the group (7) which comprise the universal invariant of this group

$$J = \left(r, \frac{w}{v}\right),$$

in common notations (in physical variables) –

$$J = \left(r, \frac{H_r}{H_z}\right).$$

## 5. DISCUSSION AND CONCLUSION

It is interesting to note that if in systems of equations (1) and (5) we transfer to new variables representing basis scalar invariants of the appropriate groups of transformations (these new variables may be called group variables), the number of equations in these systems can be reduced. In particular, the system (1) will transfer to the system of four equations for four unknown values $\varsigma_1 = E_\varphi / H_z$, $\varsigma_2 = H_r / H_z$, $\Delta\varphi_1 = \varphi_{H_z} - \varphi_{E_\varphi}$, and $\Delta\varphi_2 = \varphi_{H_z} - \varphi_{H_r}$, and system (5) - to the system

$$\frac{\partial \varsigma_1}{\partial r} = -\frac{\varsigma_1}{r} + \frac{\omega}{c} Sin\left(\Delta\varphi_1\right) + \frac{4\pi\sigma}{c}\varsigma_1^2 Cos\left(\Delta\varphi_1\right);$$

$$\frac{\partial \Delta\varphi_1}{\partial r} = \frac{4\pi\sigma}{c}\varsigma_1 Sin\left(\Delta\varphi_1\right) + \frac{\omega}{c\varsigma_1} Cos\left(\Delta\varphi_1\right),$$

where the number of equations (respectively the number of unknown values) is reduced by half. Like this, the last two equations are most convenient for their subsequent computational solution by means of known methods of the finite difference solution of differential equations (for example, by means of implicit diagram with a half weight), of course, on condition of the correct assignment of these or those boundary conditions. The matter is that in its classical type equations of an electromagnetic field (5) do not admit the computational solution by any standard methods of explicit diagram – Euler, Runge-Kutta, Adams and their varieties as the first derivatives of values $\varphi_{E_\varphi}$, $H_z$, and $\varphi_{H_z}$, and so the right parts of appropriate equations of the system (5) address in zero on the axis of plasmoid.

## REFERENCES

[1] Ovsyannikov L.V. Group analysis of differential equations (in Russian). Moscow: Nauka, 1986.

[2] Kirpichnikov A.P. Limit relations for HF inductive discharge (in Russian)//Izvestiya VUZov. Fizika. 1993. No. 1. P. 56 – 61.

[3] Kirpichnikov A.P. The structure of quasistationary electromagnetic field of high-frequency inductive discharge near an axis of plasma bunch (in Russian)//Teplofizika Vysokikh Temperatur (High Temperature). 1995. V. 33 . No. 1. P. 139 – 140.

[4] Kirpichnikov A.P. About the structure of high-frequency inductive discharge at atmospheric pressure near an axis of plasma bunch (in Russian)//Teplofizika Vysokikh Temperatur (High Temperature). 1996. V. 34 . No. 6. P. 989 – 990.

# Low Noise Microwave amplifiers with improved input matching applicable in active array antennas

M. P. Tonev

Technical University of Sofia, Bulgaria
Faculty of Tlecommunication, TU-Sofia, "Kl.Ohridsky" str. 8, 1000 Sofia, Bulgaria
E-mail: mihail_tonev@abv.bg

**Abstract**

*The difference between the optimal input reflection coefficient for achieving minimal noise figure and those needed for perfect matching is usually a challenge for low noise amplifiers design. Normally amplifiers designed to achieve lowest possible noise figure have very poor input reflection coefficient. This may cause a lot of problems in case of their application as a component in modern active phased array antennas and can be a reason for significant performance degradation. One of the possible solutions is to use balanced amplifier configuration in order to improve input and output matching. The main disadvantages of this solution are degradation of the noise figure due to the losses in the input hybrid and a bigger occupied space.*

*Another approach for solving the problem is presented in this paper. The non – unilateral properties of the transistors are used in order to obtain minimum noise figure and at the same time conjugate matching. Practical circuits and achieved performance are discussed in details.*

## 1. INTRODUCTION

As known in general for every radio-communications receiver first stage of input amplifier is matched to achieve minimal noise figure. This often leads to poor input return loss of the receiver and when it is directly connected to the receiving antenna may cause problems [5]. Usually microwave antennas are designed to be matched at their output to 50 ohms. When they see different impedance, for example as those of poorly matched low-noise amplifier, their characteristics might be changed. This is true especially concerning phased antenna arrays. Good example for such mismatch sensitive system is active antenna arrays used in modern mobile satellite communications. Such type of antennas must provide dynamic polarization control while on move. In order to support such functionality antennas must comprise dual port antenna elements receiving signals with two orthogonal linear polarizations and two independent summation feed circuits. In order to achieve good isolation between these summation circuits and to avoid phase and amplitude errors in antenna aperture it is need to ensure good matching between all feed line components inside the

antenna. So if low noise amplifiers at the antenna outputs are not well matched to their characteristic impedance it may cause significant degradation of the most important antenna parameters, such as gain and cross-polarization isolation. Two possible solutions of the mentioned above problem are known in practice. The first possible solution is to connect isolator between antenna and the receiver [2]. This completely solves the problem with poor input matching of the receiver but degrades its nose figure performance because of the insertion loss introduced by the isolator. From another side using isolator with low insertion loss will significantly increase price of the device, which is another factor that restrict using isolators. Another less expensive solution is to use balanced amplifiers [6]. Balancing technique is well known method for improving return loss of low noise amplifiers, but it also degrades noise performance due to the input hybrid device loss. Other disadvantages of balanced amplifiers are twice bigger power consumption and twice bigger occupied space compared to single ended amplifier. These disadvantages sometimes can make them not applicable.

Another approach, using a novel matching technique allowing achieving simultaneously low noise figure and good matching for such type of amplifiers is described in the presented paper.

## 2. MICROWAVE TRANSISTOR AS TWO PORT NETWORK

At microwave frequencies transistors are usually presented as two port networks, which are characterized with S-parameters [1]. Such two port network with defined load and source impedances is presented schematically on Fig.1.

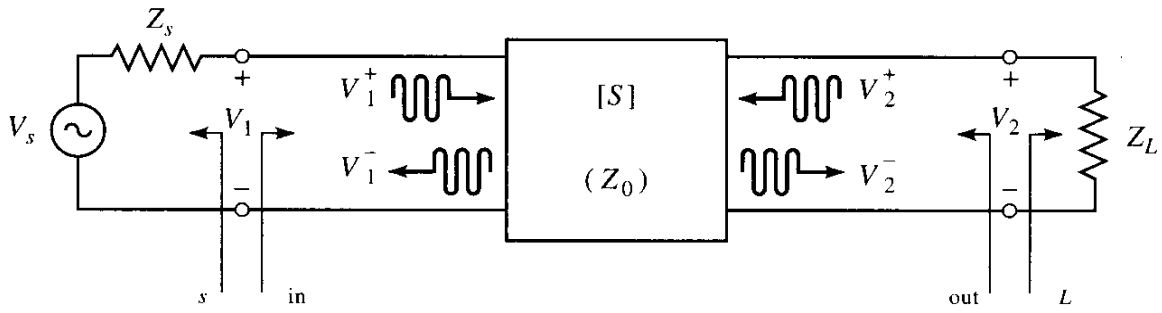


Figure.1 Two-port network with specific source and load impedances.

The three types of power gains for an arbitrary two-port network connected to source and load impedances, $Z_S$ and $Z_L$ may be defined as follows [3]:

- Power Gain = $G = P_L/P_{in}$ is the ratio of power dissipated in the load $Z_L$ to the power delivered to the input of the two-port network. This gain is independent of $Z_S$.
- Available Gain = $G_A = P_{avn}/P_{avs}$ is the ratio of the power available from the two-port network to the power available from the source. It depends on $Z_S$ but not on $Z_L$.
- Transducer Power Gain = $G_T = P_L/P_{avs}$ is the ratio of the power dissipated in the load to the power delivered to the input of two port network. This depends on both $Z_S$ and $Z_L$.

These definitions differ primarily in the way the source and load are matched to the two-port device. If the input and output are both conjugate matched, then the gain is maximized and $G = G_A = G_T$. Equations for these gains and reflection coefficients in terms of the $S$ parameters of the active device can be defined, referring to Fig.1, as follows [1]:

$$G = \frac{P_L}{P_{in}} = \frac{|S_{21}|^2 \left(1-|\Gamma_L|^2\right)}{\left(1-|\Gamma_{in}|^2\right)|1-S_{22}\Gamma_L|^2} \tag{1}$$

$$G_A = \frac{P_{avn}}{P_{avs}} = \frac{|S_{21}|^2 \left(1-|\Gamma_S|^2\right)}{|1-S_{11}\Gamma_S|^2 \left(1-|\Gamma_{out}|^2\right)} \tag{2}$$

$$G_T = \frac{P_L}{P_{in}} = \frac{|S_{21}|^2 \left(1-|\Gamma_S|^2\right)\left(1-|\Gamma_L|^2\right)}{|1-\Gamma_S\Gamma_{in}|^2 \, |1-S_{22}\Gamma_L|^2} \tag{3}$$

where

$$\Gamma_L = \frac{Z_L - Z_0}{Z_L + Z_0}, \; \Gamma_S = \frac{Z_S - Z_0}{Z_S + Z_0} \tag{4}$$

and

$$\Gamma_{in} = \frac{Z_{in} - Z_0}{Z_{in} + Z_0} = S_{11} + \frac{S_{12}S_{21}\Gamma_L}{1-S_{22}\Gamma_L} \tag{5a}$$

$$\Gamma_{out} = \frac{Z_{out} - Z_0}{Z_{out} + Z_0} = S_{22} + \frac{S_{12}S_{21}\Gamma_S}{1-S_{11}\Gamma_S} \tag{5b}$$

In general to obtain good input matching it is necessary input reflection coefficient of two port network $\Gamma_{in}$ to be close to zero. From equation 5a can be seen that $\Gamma_{in}$

depends on active component parameters ($S_{11}$, $S_{21}$, $S_{12}$) and on load reflection coefficient $\Gamma_L$. This means that we can manipulate input reflection coefficient of two port network by changing load impedance.

## 3. DESIGN OF MICROWAVE LOW NOISE AMPLIFIER WITH IMPROVED INPUT MATCHING

The main goal in designing low nose amplifiers is obtaining proper reflection coefficient from input matching network. This coefficient must coincide with optimum reflection coefficient for obtaining minimum noise figure of active component. Usually this coefficient is different from conjugate machining and this is the reason $\Gamma_{in}$ of LNA's not to be zero. It is possible to design proper input matching network and then to choose load impedance, which will minimize input reflection coefficient of the two port network. In this case amplifier will be simultaneously matched for obtaining minimum nose figure and conjugate matched with source. In general for single stage amplifier this will worse output matching. The problem can be solved by adding second stage in amplifier configuration. Then using inter-stage matching circuit we can chose proper reflection coefficient to make $\Gamma_{in} = 0$ and then output matching circuit can be designed to make $\Gamma_{out} = 0$.

The approach, presented above was proven by designing microwave LNA, suitable for using in Ku band satellite communications working in frequency band from 10.7GHz to 12.8GHz. It was designed on Arlon 25N substrate with 0.51mm thickness, dielectric constant 3.38 and loss tangent 0.0025. Used transistors are NE3210 low noise hetero-junction FET, manufactured by NEC. The S-parameters of transistors and capacitors, provided by manufacturers were putted in simulator and circuit simulation was performed.

The first step in design is to define input matching circuit. In Fig.2 reflection coefficients of input matching circuit and optimum reflection coefficient of transistor are shown. As can be seen, there is coincidence between them which means that transistor is matched for obtaining minimum noise figure. Once input of the amplifier is matched, the inter-stage and output matching circuit can be designed, using optimization procedure in order to achieve good input and output matching. Simulated S-parameters and noise figure of LNA model are shown in fig.3 and fig4.

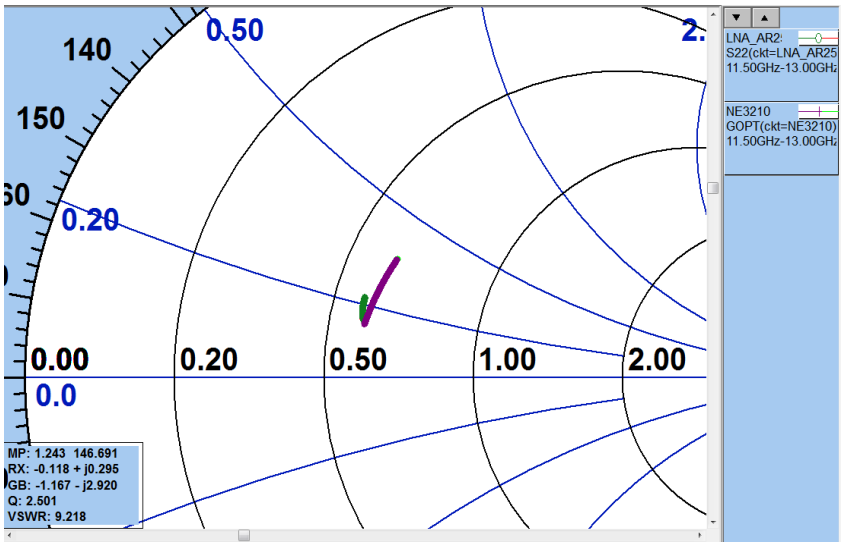


Figure.2 Reflection from input matching circuit and transistor $\Gamma_{opt}$

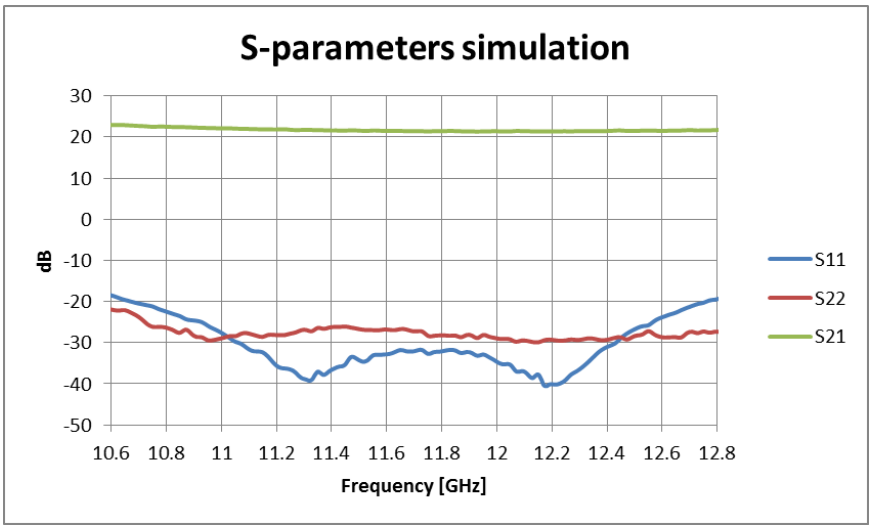


Figure.3 Simulated S-parameters of LNA

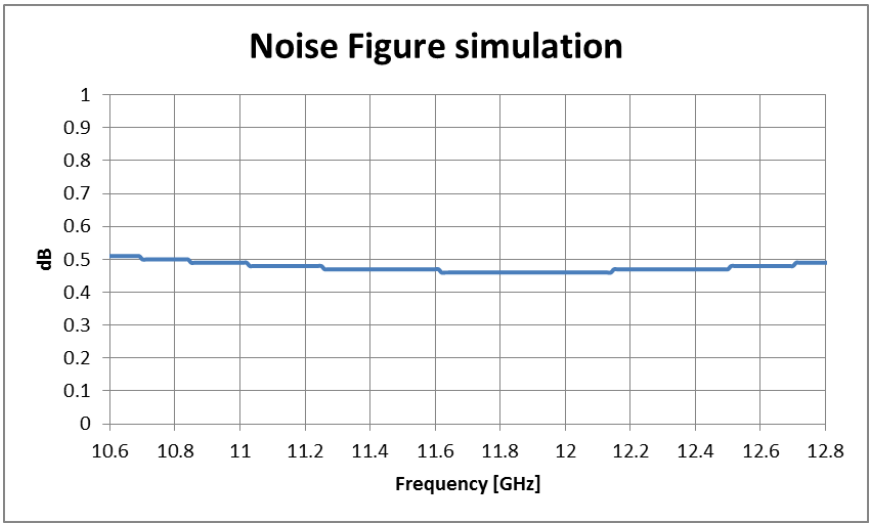


Figure.4 Simulated noise Figure of LNA

The input and output reflection coefficients are lower than 0.1 and noise figure is lower than 0.5dB. Simulated amplifier has low noise figure and good matching with source and load. To gain real inside how circuit works the simulated layout of amplifier was manufactured and measured. Measurement results are presented graphically in Fig.5 and Fig.6. Some difference between measured and simulated results may be caused by the tolerances in component parameters and by reflections from input and output connectors used for measurements. Measured input reflection coefficient is lower than 0.13 and measured noise figure is about 0.65dB.

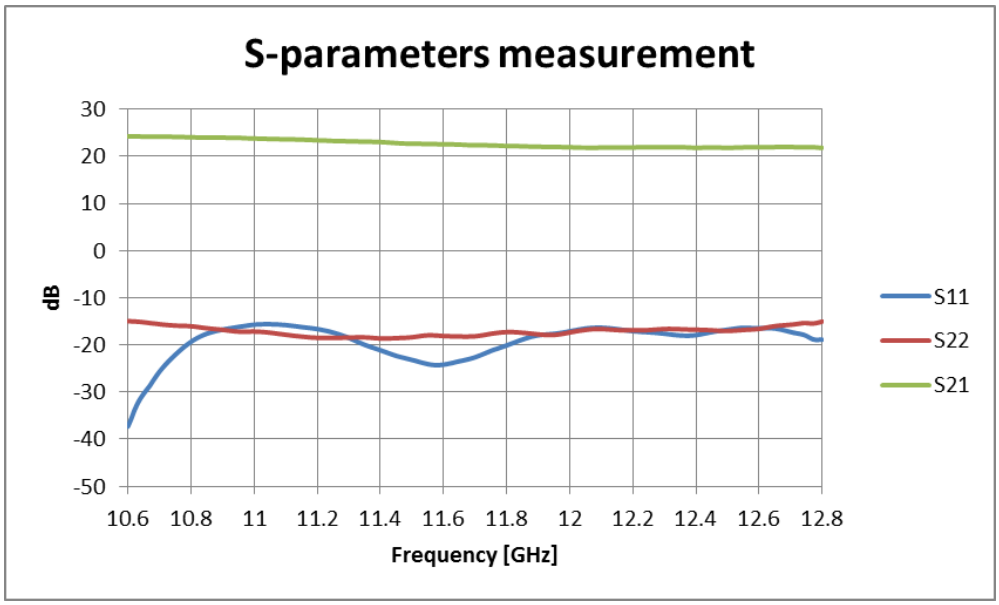


Figure.5 Measured S-parameters of LNA

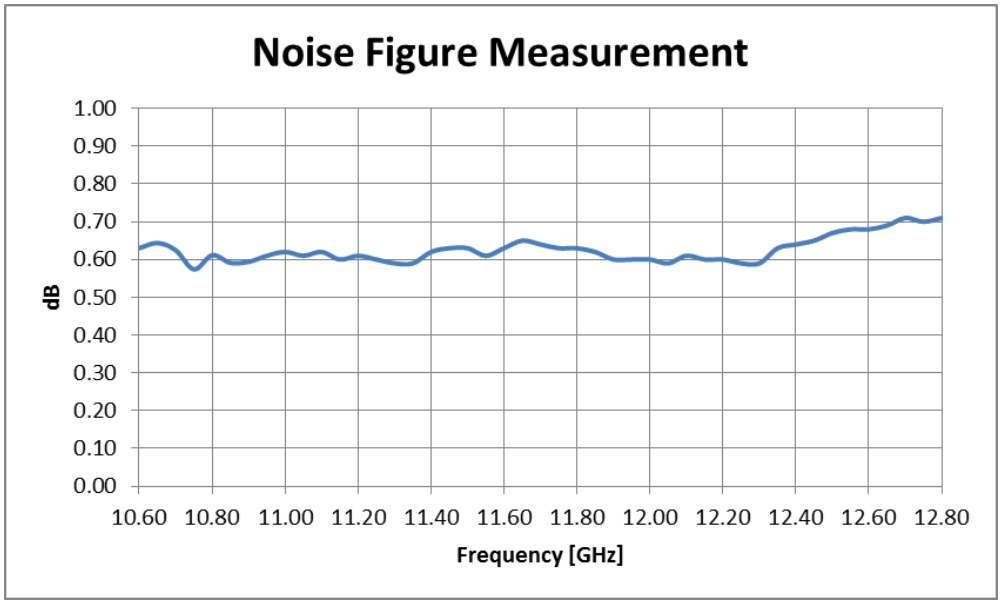


Figure.6 Measured noise Figure of LNA

## 4. CONCLUSION

A design of microwave low-noise amplifier with improved input matching was presented in this paper. As was explained this is critical parameter for some communication systems. Practically the proposed method for enhancing this parameter, by using non-unilateral characteristic of microwave transistors was proved by model measurements.

## REFERENCES

[1] Pozar, “Microwave Engineering”, 4th edition.

[2] Vendelin Rohde, Pavio, “Microwave circuit design using linear and nonlinear techniques”.

[3] Gilmore, “Practical RF Circuit Design for Modern Wireless Systems’, vol. 2.

[4] Rohde, “Microwave Circuit Design for Wireless Applications”.

[5] Pozar, “Microwave and RF Design of Wireless Systems”.

[6] Guillermo Gonzalez, “Microwave Transistor Amplifiers Analysis and Design”.

[7] Engberg, “Noise Theory of Linear and Nonlinear Circuits”.

[8] Butterworth, “High Frequency and Microwave Engineering”.

# PROVIDING A QUALITY RECEPTION OF DVB-T SIGNALS

L. Jordanova, G. Karpov, D. Dobrev

Technical University of Sofia
8, Kl.Ohridski, str.1000 Sofia, Bulgaria
jordanova@tu-sofia.bg

**Abstract**
*The paper deals with the influence of channel coding and modulation, transmitter parameters, distance between transmitter and receiver and propagation losses on the quality of received video information in DVB-T systems. Expressions for calculating of minimum carrier-to-noise ratio at the input of DVB-T receiver, necessary for quasi-error-free reception, are given. Mathematical models to determine the dependence of field strength from distance to DVB-T transmitter are presented. The dependence of minimum mean field strength at the receiver input from CNR is derived and the algorithm for determination of maximum distance to the transmitter is described.*

*This paper is a revised and expanded version of a paper entitled "Design of Radio Channel for DVB-T system" presented at CEMA 2014 International Conference, Sofia, Bulgaria, 16 - 18 October 2014.*

## 1. INTRODUCTION

As is known, required quality of the received digital TV programs is achieved when BER at the input of MPEG-4 demultiplexer is less than $10^{-11}$. This criteria corresponds to Quasi Error Free (QEF), it means less than one uncorrected error event per hour of system's work [1]. In DVB-T systems the criteria for QEF receiving can be achieved by using two-step Reed-Solomon - convolutional channel coding and COFDM method of transmitting the signal through radio channel [2].

For evaluating the quality of received TV programs in DVB-T system, three different criteria are used: the carrier-to-noise ratio (CNR) at the receiver input required for QEF reception, the available useful data rate and the field strength required for different reception modes. There are four reception modes, namely, fixed reception with rooftop antenna, portable outdoor and indoor reception and mobile reception.

The aim of this research is to derive relationships for determination of minimum CNR and its corresponding field strength at the receiver input that is required for QEF reception, taking into account the parameters of DVB-T transmitter and receiver, the distance between them and the communication channel parameters.

## 2. CARRIER-TO-NOISE RATIO AT THE RECEIVER INPUT DEPENDING ON CODE PARAMETERS AND MODULATION TYPE

To determine CNR values, that are required to achieve QEF reception, it is necessary BER characteristics of DVB-T channel for different convolutional code rates and modulation types to be known.

In DVB-T systems the MPEG-4 digital stream is firstly applied to the input of RS-coder and then, RS-coded stream is applied to the input of convolutional coder. The used Reed-Solomon code RS(204, 188, t = 8) allows to correct up to 8 error bytes in a block and its rate is $R_{RS}$ = 188/204 = 0.92. The rate of the basic convolutional code is $R_C$ = 1/2, as by puncturing operation the following higher rates could be achieved: 2/3, 3/4, 5/6, 7/8.

For transmitting of payload digital stream (video, audio signals and additional programs data) plus bits for error protection and synchronization bits, the DVB-T standard uses two modes – 2K with 1512 subcarriers and 8K with 6048 subcarriers. Subcarriers are equally distributed through the baseband of one TV channel, which is 8 MHz. The used methods for modulation of subcarriers are QPSK, 16-QAM and 64-QAM.

### 2. 1. Error probability in DVB-T channel

The bit error probability (BEP) after convolutional decoder $P_{C,out}$ depends on parameters of transmitted signal, and on the characteristics of the communication channel. The upper bound of BEP after convolutional decoder is defined as [3]

$$P_{C,out} \le \frac{1}{k} \sum_{d=d_{free}}^{\infty} w(d) P_d \left( E_b / N_0 \right), \tag{1}$$

where $P_d(E_b/N_0)$ is the probability of choosing an incorrect path at Viterbi decoding, which differs from the correct path in terms of $d$ positions, $k$ is the constructive code length, $d$ is the free distance of convolutional code, $w(d)$ is the number of paths with

distance $d$, $d_{free}$ specifies the free distance of the used code. Values of parameters $d$ and $w(d)$ are given in [4].

For Rayleigh fading channel there is the following dependence between probability $P_d$ and BEP in communication channel $P_{in}$ [5]:

$$P_d = P_{in}^d \sum_{k=0}^{d-1} \binom{d-1+k}{k} (1-P_{in})^k . \tag{2}$$

BEP in communication channel, used for transmitting the M-QAM modulated signal, is defined as [6]

$$P_b\left(E_b/N_0\right) = \frac{2}{\log_2 M}\left(1-\frac{1}{\sqrt{M}}\right)\left(1-\frac{1}{K}\right)-\left(1-\frac{1}{\sqrt{M}}\right)^2\left(1-\frac{4}{\pi}\cdot\frac{1}{K\cdot \mathrm{tg}(K)}\right) , \tag{3}$$

where $K = (M - 1 + x)/x$ and $x = 1.5\cdot(E_b/N_0)\cdot R_{RS}\cdot R_C\cdot\log_2(M)$.

The bit error probability after the RS decoder $P_{RS,out}$ is related to the bit error probability at the input of RS decoder $P_{RS,in}$ by the following dependence [4]:

$$P_{RS,out} = \frac{1}{N\log_2 M}\sum_{i=t+1}^{N} \beta_i \binom{N}{i} \times \left(P_{RS,in}\log_2 M\right)^i \left(1-P_{RS,in}\log_2 M\right)^{N-i} , \tag{4}$$

where $N$ is the number of symbols in a RS-coded block ($N = 204$), $t$ is the maximal number of erroneous symbols, that can be corrected with RS code ($t = 8$), $\beta_i$ is the average number of symbol errors remaining uncorrected in the received block after decoding. According to DVB-T standard it is accepted that $\beta_i = i$. In formula (4) $P_{RS,in}$ actually represents BEP after the convolutional decoder.

## 2. 2. BER characteristics of DVB-T channel

To estimate the noise immunity of DVB-T channel the dependence of BER at channel decoder output from CNR at demodulator input is used. The relation between CNR and $E_b/N_0$, expressed in dB, is given by [2]

$$CNR = \frac{E_b}{N_0} + 10\lg m - 10\lg\left(1-\alpha/4\right) + 10\lg\left(R_{RS}R_C\right) + 10\lg\frac{N_{pl}}{N_{nz}} + 10\lg\frac{T_s}{T_s+T_\tau} , \tag{5}$$

where $m = \log_2 M$ is the number of bits per symbol; $\alpha$ is the roll-off factor of $\sqrt{\cos^2}$-filter ($\alpha = 0{,}35$); $N_{pl}$ is the number of subcarriers, used to carry payload information; $N_{nz}$ is the number of non-zero subcarriers, used to carry TPS (Transmission Parameter Signaling), pilot carriers and data; $T_s$ is the period of one OFDM symbol and $T_\tau$ is the guard interval length.

The influence of modulation type and convolutional code rate on the noise immunity of DVB-T channel is shown on figure 1. In this simulation research is

accepted that $k = 6$, $N_{pl} = 6048$, $N_{nz} = 6817$ and $T_\tau = T_s/32$. From this figure the values of CNR, that are required to achieve BER = $10^{-11}$, could be easily accounted. It is evident that increasing the modulation level in order to achieve higher transmission rates through radio channel requires working at lower convolutional code rates.

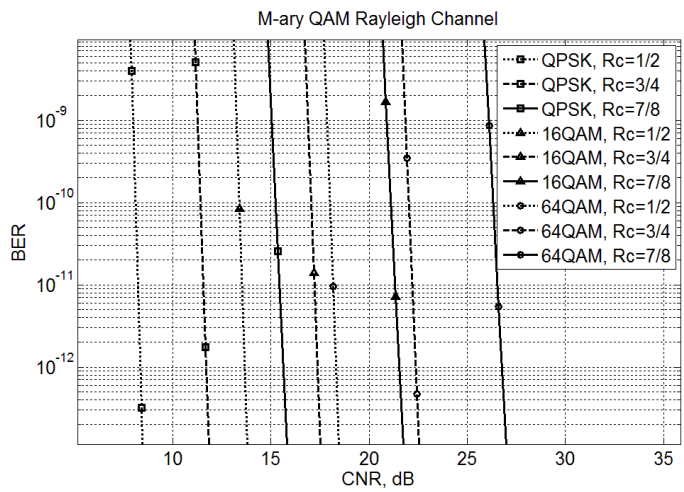


Figure 1. BER dependences for different modulations and convolutional code rates.

The influence of OFDM symbol guard interval on the channel noise immunity can be estimated from figure 2. It can be seen that in order to maintain a certain quality of reception, when $T_\tau$ decreases from $T_s/4$ to $T_s/32$, it is necessary to increase CNR by 1 dB. Moreover, the system spectral efficiency increases, because the data transmission rate is higher at lower values of $T_\tau$.

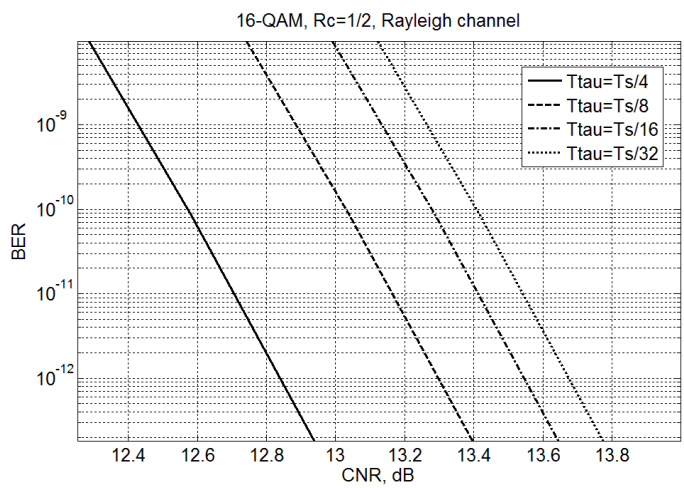


Figure 2. Impact of OFDM guard interval length on the noise immunity of DVB-T channel for 16QAM and $R_C = 1/2$.

Dependences, given in this section are used for calculation of minimum acceptable values of parameter CNR for Rice and Rayleigh channels, when reception is fixed

(FR), portable outdoor (PO), portable indoor (PI) and mobile (MO). Obtained values of CNR (in dB) are given in table 1.

Table 1. Acceptable values of CNR

| Modulation | $R_C$ | Race channel | Rayleigh channel | |
|---|---|---|---|---|
| | | FR | PO/PI | MO |
| QPSK | 1/2 | 5.9 | 8.2 | 11.1 |
| QPSK | 2/3 | 7.9 | 10.2 | 13.2 |
| QPSK | 3/4 | 9.1 | 11.6 | 14.5 |
| QPSK | 5/6 | 10.3 | 12.8 | 15.8 |
| QPSK | 7/8 | 11.3 | 15.4 | 16.9 |
| 16-QAM | 1/2 | 11.6 | 13.5 | 16.8 |
| 16-QAM | 2/3 | 14.1 | 16.4 | 19.4 |
| 16-QAM | 3/4 | 15.7 | 17.2 | 21.1 |
| 16-QAM | 5/6 | 16.9 | 19.4 | 22.4 |
| 16-QAM | 7/8 | 17.5 | 21.3 | 23.1 |
| 64-QAM | 1/2 | 17.2 | 18.1 | 22.4 |
| 64-QAM | 2/3 | 19.5 | 21.8 | 24.8 |
| 64-QAM | 3/4 | 21.2 | 22.2 | 26.6 |
| 64-QAM | 5/6 | 22.7 | 25.2 | 28.2 |
| 64-QAM | 7/8 | 23.7 | 26.6 | 29.3 |

## 3. ACCEPTABLE FIELD STRENGTH AT THE RECEIVER INPUT

Large numbers of experimental and theoretical researches were conducted with purpose to find the dependence of field strength at the receiver input from minimum CNR, at which the QEF reception is provided. Obtained results for different conditions were described in detail and documented in resolutions of Regional Radio communication Conference (RRC-06) of ITU-R.

The following dependence was derived to determine the minimum field strength at receiving place $E_{\min}$ (in dBμV/m), necessary for QEF reception [2]:

$$E_{\min} = P_{r\,\min} - G_r - 10\lg\left(\frac{1.64\lambda^2}{4\pi}\right) + L_f\,, \tag{6}$$

where $P_{r\,\min}$ is the acceptable minimum signal level at the DVB-T receiver input in dBW, $G_r$ is the receiver antenna gain related to half-dipole in dBi, $\lambda$ is the receive signal wave length in m and $L_f$ is the receiver feeder losses in dB.

The minimum level of receive signal is limited by acceptable values of CNR (see Table 1) and noise power $P_n$ at the receiver input, i.e.

$$P_{r\,\min} = \mathrm{CNR} + P_n\,. \tag{7}$$

To calculate the value of $P_n$ the following equation can be used:

$$P_n = 10\lg(k) + 10\lg(B_n) + 10\lg(T) + NF_r\,, \tag{8}$$

where $k = -1.38.10^{-23}$, W/K.Hz is the Boltzmann's constant, $B_n$ is the receiver noise bandwidth in Hz (for channel bandwidth 8 MHz $B_n$ = 7,61 MHz) , $T$ = 290 K is the absolute temperature and $NF_r$ is hte receiver noise figure in dB (according to ITU-R recommendations for DVB-T receivers $NF_r$ = 7 dB).

For design of DVB-T channel the minimum mean field strength at the receiving place $E_{\text{med}}$ is used. Except on $E_{\text{min}}$, it depends on the receiving mode and is calculated using following expressions:

$$E_{\text{med}} = E_{\text{min}} + P_{\text{mmn}} + C_l \ - \ \text{FR mode} \tag{9}$$

$$E_{\text{med}} = E_{\text{min}} + P_{\text{mmn}} + C_l + L_h \ - \ \text{PO and MO mode} \tag{10}$$

$$E_{\text{med}} = E_{\text{min}} + P_{\text{mmn}} + C_l + L_h + L_b \ - \ \text{PI mode} \tag{11}$$

Coefficients used in these expressions, whose values are given in dB, account influence of following factors: man-made noise ($P_{\text{mmn}}$); characteristics of area of receiver location ($C_l$); losses from changing the height of receiver antenna relative to the reference value, that is accepted to be 1.5 m above ground level ($L_h$) and mean building entry loss ($L_b$).

Dependences of mean minimum field strength in receiving place $E_{\text{med}}$ (in dBμV/m) from minimum CNR value at the receiver input (in dB) for fixed reception with rooftop antenna, portable outdoor reception and portable indoor reception are shown on figure 3. To obtain these dependences it is accepted that $f$ = 600 MHz, $G_r$ = 11 dBi, $L_f$ = 4 dB the recommended by ITU-R values of coefficients in expressions (9) - (11) are used: $P_{\text{mmn}}$ = 0 dB, $L_h$ = 17 dB, $L_b$ = 8 dB and $C_l$, that depends on the location probability and can be 13 dB (99%), 9 dB (95%) and 3 dB (70%) [7].

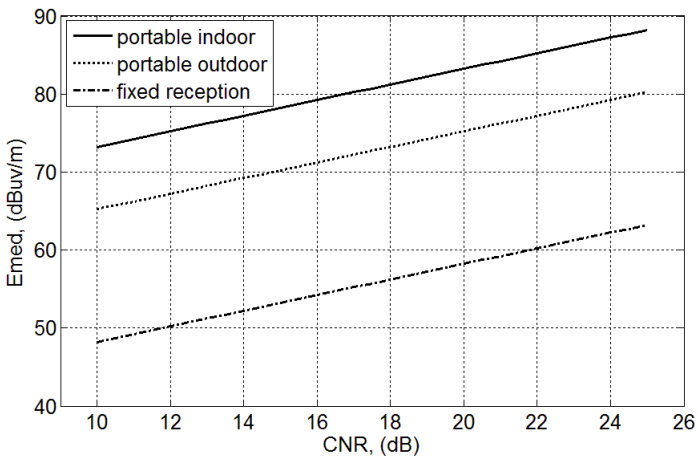


Figure 3. Minimum median field strength corresponding to the minimum CNR for 95% location probability

Using obtained dependences easily can be found the values of $E_{\text{med}}$ at the receiver input, necessary for QEF reception for different parameters of DVB-T signal and different reception conditions. For example, if modulation of subcarriers in OFDM symbol is 16QAM, convolutional code rate is $R_C = 3/4$, from table 1 the following values of CNR are obtained: 15.7 dB (fixed reception) and 17.2 dB (portable indoor and outdoor reception). To ensure these values of CNR it is necessary the field strength at receiving place $E_{\text{med}}$ to be not less then 53.9 dBμV/m – for fixed reception, 72.4 dBμV/m – for portable outdoor reception and 80.4 dBμV/m – for portable indoor reception.

## 4. DEPENDENCE OF FIELD STRENGTH FROM DISTANCE TO TRANSMITTER

To calculate the field strength, created by the transmitter at the receiver input $E$ in dBμV/m, the following relationship can be used:

$$E = \Phi + 120 + 10\lg\left(Z_{c0}\right) = \text{EIRP} - L + 20\lg f + 107.21, \tag{12}$$

where $\Phi$ is the power flux density at the receiving point in dBW/m$^2$, $Z_{c0} = 120\pi$ is the free space wave impedance, EIRP is the equivalent isotropic radiated power of transmitter in dBW, $L$ is the propagation loss from transmitter to receiver in dB and $f$ is the signal frequency in MHz.

If the output transmitter power $P_t$ (in W) is given, the following expression is used to calculate EIRP in dBW:

$$\text{EIRP} = 10\lg\left(P_t\right) + G_t - L_\Sigma \tag{13}$$

where $G_t$ is the gain of transmitter antenna in dBi and $L_\Sigma$ is the transmitter feeder losses in dB.

For determining the propagation loss in communication channel $L$ it is necessary to choose an adequate model, describing the radio signal propagation in high and middle populous urban zones. There are several models which are based on data of the empirical Okumura model. This model is considered as most precise model but it is presented by tabulated values and is not enough suitable for design.

Semi-empirical model of Hata, presented by the group of dependences, describing radio signal propagation losses in different conditions is a good solution for developers' purposes. The range of input values in Hata model is extended against Okumura model input value range, but is not enough for universal use of the model.

There are some modifications of Hata model for more extent ranges of input parameter values. The most precise and used are ITU-R P.529-3 and ERC 68 modifications of Hata models.

### 4. 1. Propagation loss

In this work for determination of propagation loss in DVB-T channel for urban (U), sub-urban (SU) and open (O) zones Hata-Okumura and P.529-3 models are used, that are applicable under the following conditions: frequency range – from 150 MHz to 1500 MHz, transmitter antenna height – from 30 m to 200 m, receiver antenna height – from 1 m to 10 m and distance between the transmitter and receiver – from 1 km to 20 km (Hata model) and from 1 km to 100 km (P.529-3 model). These models are suitable for 50% of coverage zone within 50% of time.

The Hata expression for propagation loss $L$ (in dB) in urban zone is

$$L = 69.55 + 26.16\lg(f) - 13.82\lg(h_t) - \alpha(h_r) + \left[44.9 - 6.55\lg(h_t)\right]\lg(d) \tag{14}$$

where $f$ is the working frequency in MHz, $h_t$ is the transmitter antenna height in m, $h_r$ is the receiver antenna height in m, $\alpha(h_r)$ is the receiver antenna height correction in dB, $d$ is the distance between transmitter and receiver in km.

In the case of large city and $f \geq 400$ MHz

$$\alpha(h_r) = 3.2\left[\lg(11.75\,h_r)\right]^2 - 4.97\,. \tag{15}$$

Modified model ITU-R P.529-3 for determination of propagation loss in dB has the following form [8]:

$$L = 69.82 + 6.16\lg(f) - 13.82\lg(h_t) - \alpha(h_r) + \left[44.9 - 6.55\lg(h_t)\right]\lg(d)^b\,. \tag{16}$$

The receiver antenna height correction factor is computed as

$$\alpha(h_r) = \left[1.1\lg(f) - 0.7\right]h_r - \left[1.56\lg(f) - 0.8\right]. \tag{17}$$

The value of index $b$ for $d \leq 20$ km is 1, and for $d > 20$ km is calculated by the following formula:

$$b = 1 + \left(0.14 + 1.87\,f \cdot 10^{-4} + 1.07\,h_t^* \cdot 10^{-3}\right)\left[\lg(d/20)\right]^{0.8} \tag{18}$$

where

$$h_t^* = h_t \Big/ \left(1 + 7\,h_t^2 \cdot 10^{-6}\right)^{1/2}. \tag{19}$$

### 4. 2. Simulation study

The figures shown below illustrate the dependence of the field strength at the reception point $E$ (dBμV/m) on the distance between the transmitter and the receiver

*d* (km) when changing the height of the transmitter and receiver antennas and the output power of the transmitter. To determine the propagation loss *L* both models are used: empirical Hata model, when *d* is from 1 to 20 km and modified Hata model ITU-R P.529-3 – for *d* = 20 - 55 km.

The study shows, that with increasing the transmitter antenna height $h_t$ the gain in the received signal power decreases and at $h_t > 200$ m becomes smaller than 2 dB. The increase of the receiver antenna height $h_r$ with each 3 m leads to 5 dB gain in the received signal power.

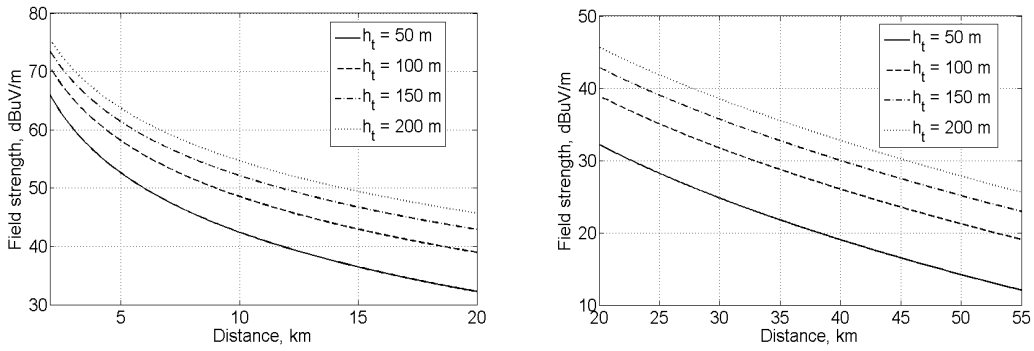


*a*) *b*)

Figure 4. Dependences of *E* on *d* for $P_t = 1$kW, $f = 600$MHz, $h_r = 1.5$ m and different transmitter heights: *a*) Hata-Okumura model, *b*) P.529-3 model.

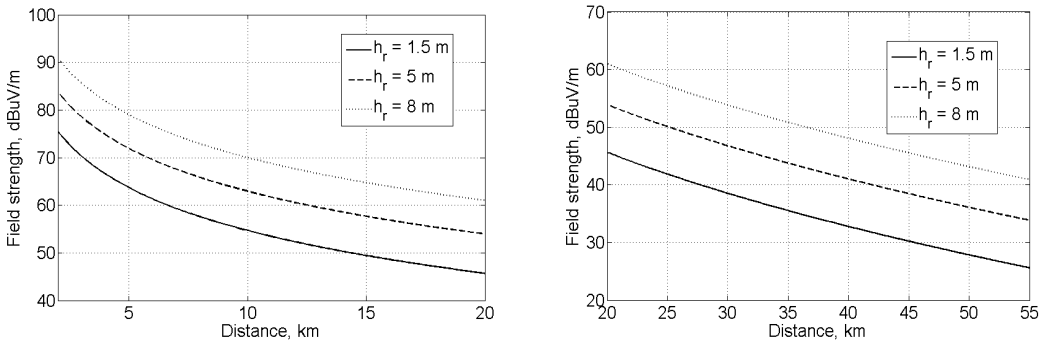


*a*) *b*)

Figure 5. Dependences of *E* on *d* for $P_t = 1$kW, $f = 600$MHz, $h_t = 200$ m and different receiver antenna heights: *a*) Hata-Okumura model, *b*) P.529-3 model.

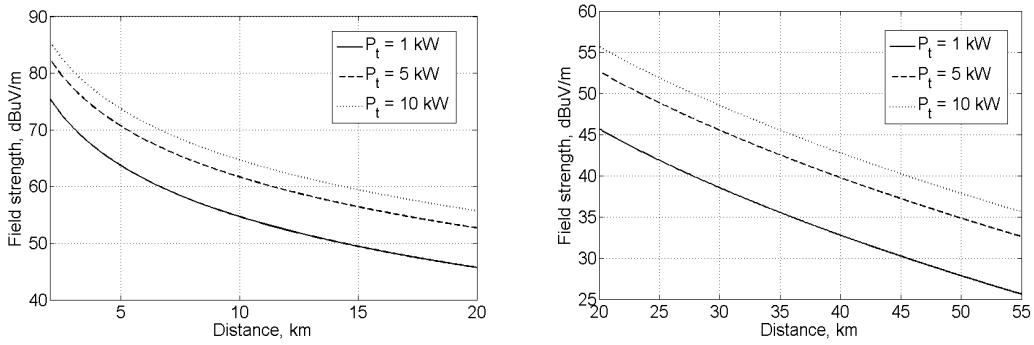


*a*) *b*)

Figure 6. Dependences of $E$ on $d$ for $f = 600$ MHz, $h_r = 1.5$ m, $h_t = 200$ m and different transmitted powers: *a*) Hata-Okumura model, *b*) P.529-3 model.

As can be seen from figure 6 the increasing of transmitted power from 1 kW to 5 kW causes 7 dB increase of the field strength at the receiver input. By increasing the transmitted power from 5kW to 10kW, the field strength at the receiving place increases with approximately 3 dB.

## 5. SERVICE ZONE OF DVB-T TRANSMITTER

Service zone of DVB-T transmitter is characterized by the field strength that is above the minimum mean field strength $E_{\text{med}}$. To determine maximum acceptable distance between transmitter and receiver $d_{\max}$, necessary for QEF reception, the dependences given in the fourth section of this publication may be used. The obtained values of $d_{\max}$ at $f = 600$ MHz for several different values of the parameters $h_t$, $P_t$ and $h_r$ are given in table 2.

Table 2. Values of $d_{\max}$ required for QEF reception, km

| Mode | $h_t$, m | | | $P_t$, kW | | | $h_r$, m | | |
|---|---|---|---|---|---|---|---|---|---|
| | 50 | 100 | 200 | 1 | 5 | 10 | 1.5 | 5 | 8 |
| FR | 4.1 km | 6.1 km | 9.45 km | 9.45 km | 16.2 km | 20.5 km | 9.45 km | 16.2 km | 20.5 km |
| PO | < 2 km | 2.2 km | 2.6 km | 2.6 km | 4.3 km | 5.5 km | 2.6 km | 4.3 km | 5.5 km |
| PI | < 1 km | < 1 km | < 2 km | < 2 km | 2.3 km | 3 km | < 2 km | 2.3 km | 3 km |

In Singe Frequency networks (SFN) the radius of the service zone of a DVB-T transmitter is limited by the maximum acceptable distance between transmitters, which is determined by the COFDM symbol guard interval. If signal from far distant transmitters are delayed more than allowed by the guard interval they behave as noise like interfering signals rather than wanted signals. The level of such signal depends on the propagation conditions, which will vary with time. As is known, the self interference of SFN for given transmitter spacing is reduced by selecting large guard

interval. The maximum distances between transmitters $d_{max}$ for different guard intervals $T_\tau$ can be calculated by the formula $d_{max} = c.T_\tau$ ($c = 3.10^8$, m/s is the light speed). For DVB-T systems operating at 8K carrier mode the obtained values of $d_{max}$ are given in table 3.

Table 3. Values of $d_{max}$ depending on the guard interval, km.

| Guard interval | 1/4 | 1/8 | 1/16 | 1/32 |
|---|---|---|---|---|
| Guard interval duration in μs | 224 | 112 | 56 | 28 |
| Distance in km | 67.2 | 33.6 | 16.8 | 8.4 |

Therefore, when determining the service area of DVB-T transmitter two demands have to be taken into account. The first one is related to the need to provide QEF reception, and the second ensures the avoidance of self interference in SFN.

## 6. CONCLUSION

Dependences for determination of field strength at receiving place, given in this publication, allow take into account parameters of DVB-T transmitter and receiver, conditions of radiated radio signal propagation and mode of its receiving. These dependences are used for development of software, used for resolving some important problems, related to design of terrestrial television networks. These problems are: determination of output power, antenna gain and antenna system directional properties for DVB-T transmitters, creating conditions for QEF reception, while changing radio signal propagation conditions and signal reception mode and other.

## REFERENCES

[1] EN 300 744, “Digital Video Broadcasting: Framing structure, channel coding and modulation for digital terrestrial television”, ETSI, 2009.

[2] W. Fischer, “Digital Video and Audio Broadcasting Technology”, Springer, 2008.

[3] J. Odanwalder, “Error Control Coding Handbook”, Linkabit Corporation, San Diego, 1996.

[4] TR 101 290, “Digital Video Broadcasting (DVB); Measurement guidelines for DVB systems”, ETSI, 2001.

[5] J. Proakis, “Digital Communications”, McGraw-Hill, 2003.

[6] K. Marvin, S. Alouini, “Digital Communication Over Fading Channels”, John Wiley & Sons, Inc., 2000.

[7] "Final acts of the RRC-06 for planning of the digital terrestrial broadcasting service in parts of Regions 1 and 3 in frequency bands 174 - 230 MHz and 470 – 862 MHz", ITU, 2006.

[8] SP 2/01, "Investigation of Modified Hata Propagation Models, Spectrum Planning Team, Australian Communications Authority, April, 2001.